NeuroImage: Clinical 23 (2019) 101919

Contents lists available at ScienceDirect

NeuroImage: Clinical

journal homepage: www.elsevier.com/locate/ynicl

A lesion and connectivity-based hierarchical model of chronic aphasia recovery dissociates patients and healthy controls

Erin L. Meier*, Jeffrey P. Johnson, Yue Pan, Swathi Kiran

Department of Speech, Language, & Hearing Sciences, Sargent College of Health and Rehabilitation Sciences, Boston University, 635 Commonwealth Avenue, Room 326, Boston, MA 02215, United States of America

ARTICLE INFO

Keywords:
Aphasia
Stroke
Lexical-semantics
Effective connectivity
Structure-function relationships

ABSTRACT

Traditional models of left hemisphere stroke recovery propose that reactivation of remaining ipsilesional tissue is optimal for language processing whereas reliance on contralesional right hemisphere homologues is less beneficial or possibly maladaptive in the chronic recovery stage. However, neuroimaging evidence for this proposal is mixed. This study aimed to elucidate patterns of effective connectivity in patients with chronic aphasia in light of healthy control connectivity patterns and in relation to damaged tissue within left hemisphere regions of interest and according to performance on a semantic decision task. Using fMRI and dynamic causal modeling, biologically-plausible models within four model families were created to correspond to potential neural recovery patterns, including Family A: Left-lateralized connectivity (i.e., no/minimal damage), Family B: Bilateral anterior-weighted connectivity (i.e., posterior damage), Family C: Bilateral posterior-weighted connectivity (i.e., anterior damage) and Family D: Right-lateralized connectivity (i.e., extensive damage). Controls exhibited a strong preference for left-lateralized network models (Family A) whereas patients demonstrated a split preference for Families A and C. At the level of connections, controls exhibited stronger left intrahemispheric task-modulated connections than did patients. Within the patient group, damage to left superior frontal structures resulted in greater right intrahemispheric connectivity whereas damage to left ventral structures resulted in heightened modulation of left frontal regions. Lesion metrics best predicted accuracy on the fMRI task and aphasia severity whereas left intrahemispheric connectivity predicted fMRI task reaction times. These results are discussed within the context of the hierarchical recovery model of chronic aphasia.

1. Introduction

Recovery from aphasia, one of the most prevalent and debilitating consequences of stroke, is notoriously difficult to predict. Personal factors (e.g., age, gender, education, socio-economic status) and traditionally-defined stroke characteristics (e.g., lesion size, lesion location) do not provide sufficient predictive power (Lazar et al., 2008). In recent years, researchers have begun to incorporate robust neuroimaging datasets into aphasia recovery models. However, despite continued advances in neuroimaging tools and techniques, emerging computational recovery models are still unable to consistently and accurately predict recovery trajectories of individual persons with aphasia (PWA) in the chronic post-stroke stage (Hope et al., 2013; Price et al., 2017). One potential reason for this lack of predictive power is that most chronic

Abbreviations: AG, Angular gyrus; aCommissure, Anterior Commissure; pole, Anterior temporal pole; AQ, Aphasia quotient; AF, Arcuate fasciculus; ART, Artifact Detection Tools toolbox; AAL, Automated Anatomical Labeling; BMA, Bayesian model averaging; BMS, Bayesian model selection; BPA, Bayesian parameter averaging; BNT, Boston Naming Test; CC, Connectivity component; CCallosum, Corpus Callosum; CVA, Cerebrovascular accident; DCM, Dynamic causal modeling; xp, Exceedance probability; exp., Exponentiated; FDR, False discovery rate; GLM, General linear model; IFGop, Inferior frontal gyrus, pars opercularis; IFGorb, Inferior frontal gyrus, pars orbitalis; IFGtri, Inferior frontal gyrus, pars triangularis; IFOF, Inferior fronto-occipital fasciculus; ILF, Inferior longitudinal fasciculus; ITG, Inferior temporal gyrus; L, Left; IntraLH, Left intrahemispheric connectivity; LC, Lesion component; MCA, Middle cerebral artery; MFG, Middle frontal gyrus; MTG, Middle temporal gyrus; PWA, Persons with aphasia; p, Posterior; PCA, Principal component analysis; PreCG, Precentral gyrus; PALPA, Psycholinguistic Assessments of Language Processing in Aphasia; PPT, Pyramids and Palm Trees Test; ROI[s], Region(s) of interest; RT, Response time; R, Right; SnPM, Statistical nonparametric mapping toolbox; STG, Superior temporal gyrus; SMA, Supplementary motor area; SMG, Supramarginal gyrus; TPC, Temporoparietal cortex; UF, Uncinate fasciculus; VOI[s], Volume(s) of interest; WAB-R, Western Aphasia Battery-Revised

* Corresponding author at: Department of Neurology, Johns Hopkins University School of Medicine, 600 N. Wolfe Street, Phipps 546C; Baltimore, MD 21287, United States of America.

E-mail address: emeier5@jhmi.edu (E.L. Meier).

https://doi.org/10.1016/j.nicl.2019.101919
Received 20 October 2018; Received in revised form 5 June 2019; Accepted 30 June 2019
Available online 02 July 2019

recovery models include structural stroke variables yet exclude critical metrics of brain function (Price et al., 2017).

By contrast, in an early theoretical model of neural reorganization in chronic aphasia, Heiss and Thiel (2006) described different behavioral recovery profiles based on combined structural and functional metrics. Specifically, the authors first posited that minimal acute damage to the language-dominant left hemisphere results in reinstatement of pre-stroke language activation patterns and optimal—or possibly complete—language recovery. Second, they proposed satisfactory (but incomplete) language recovery is the result of damage to primary, perisylvian language cortex that forces functional recruitment of the remaining undamaged extrasylvian regions for language processing. Finally, Heiss and Thiel (2006) stated that poor behavioral recovery is the consequence of extensive left hemisphere damage that renders only the contralesional right hemisphere available to mediate language.

Consistent with the Heiss and Thiel (2006) recovery hierarchy, many PET and fMRI studies in PWA (e.g., Allendorfer et al., 2012; Fridriksson, 2010; Fridriksson et al., 2010; Fridriksson et al., 2012; Heiss et al., 1999; Léger et al., 2002; Meinzer et al., 2008; Rosen et al., 2000; Szaflarski et al., 2013, 2011; van Oers et al., 2010; Warburton et al., 1999) have demonstrated that patients with the most intact speech and language abilities recruit remaining left hemisphere cortex—and perilesional tissue in particular—during language tasks. Furthermore, several studies have demonstrated that chronic patients who respond most favorably to language treatment show increased activation of left hemisphere areas from pre- to post-therapy scans (e.g., Fridriksson, 2010; Fridriksson et al., 2012; Marcotte and Ansaldo, 2010; Meinzer et al., 2008; Menke et al., 2009; Raboyeau et al., 2008; van Hees et al., 2014a; Vitali et al., 2007). Also consistent with the Heiss and Thiel (2006) proposition are studies that have demonstrated that the right hemisphere is insufficient for language processing in patients with chronic aphasia or possibly even maladaptive for continued recovery from the disorder (Belin et al., 1996; Blank et al., 2003; Naeser et al., 2004; Postman-Caucheteux et al., 2010; Price and Crinion, 2005; Richter et al., 2008; Warburton et al., 1999). On the other hand, persistent right hemisphere (or bilateral) activation has also been found in chronic patients with good language skills (Abo et al., 2004; Blasi et al., 2002; Breier et al., 2006; Cao et al., 1999; Cherney and Small, 2006; Mattioli et al., 2014; Mohr et al., 2014; Musso et al., 1999; Raboyeau et al., 2008). In the same vein, patients who suffered a second, right hemisphere infarct subsequent to initial left hemisphere stroke have been shown to present with worsened aphasia (Barlow, 1877; Basso et al., 1989; Cappa and Vallar, 1992; Levine and Mohr, 1979; Turkeltaub et al., 2012), which implies that the right hemisphere can play a critical beneficial role in language processing in PWA.

A few studies studies (e.g., Griffis et al., 2017a; Griffis et al., 2017b; Heiss et al., 1999; Saur et al., 2006; Skipper-Kallal et al., 2017b, 2017a) have described distinct associations between lesion, activation, and behavior profiles that partially align with the Heiss and Thiel (2006) recovery patterns. However, empirical support for all three patterns within the same patient sample is lacking. For one, recruitment of regions outside the perisylvian language network (i.e., regions typically associated with domain-general cognition, including e.g., the middle frontal gyrus, the frontal operculum, dorsal anterior cingulate cortex, supplementary motor area, and intraparietal sulcus, see Fedorenko et al., 2011; Fedorenko et al., 2013) may in fact constitute optimal—rather than suboptimal—language activation patterns for PWA. In their meta-analysis of language activation studies in PWA, Turkeltaub et al. (2011) discovered patients with chronic aphasia activated the left middle frontal gyrus (LMFG) across a variety of language tasks, which could indicate that LMFG (or dorsolateral prefrontal cortex more generally) plays an undetermined—but possibly crucial—role in aphasia recovery. Greater activation of domain-general cortex in the subacute phase has been shown to predict language abilities by the chronic recovery stage (Geranmayeh et al., 2017). Furthermore, patients with chronic aphasia have demonstrated a reliance on domain-general networks and connectivity of domain-general regions during language tasks (Brownsett et al., 2014; Geranmayeh et al., 2016; Meier et al., 2018; Meier et al., 2016a; Sharp et al., 2010).

Given the current lack of clarity regarding beneficial activation patterns in PWA, it is perhaps no surprise that measures of brain function have been excluded from predictive models of aphasia recovery. We propose, however, that functional imaging can provide crucial information regarding aphasia recovery profiles if functional metrics capture the interconnected nature of language processing (i.e., via network connectivity methodologies) and are explicitly linked to lesion and behavioral profiles. Task-based connectivity methods have been incorporated into some recent investigations in PWA (Geranmayeh et al., 2016; Kiran et al., 2015; Sandberg et al., 2015; Sharp et al., 2010; Vitali et al., 2010; Warren et al., 2009). Other studies have included careful and explicit control of lesion location and extent when interrogating activation in patients with aphasia (e.g., Fridriksson, 2010; Fridriksson et al., 2010; Fridriksson et al., 2012; Griffis et al., 2017a; Griffis et al., 2017b; Sims et al., 2016; Skipper-Kallal et al., 2017bSkipper-Kallal et al., 2017a). To our knowledge, though, no previous study has utilized connectivity methods while accounting for patient lesion and language profiles to explicitly test whether hierarchical recovery patterns can be dileaneated in patients with chronic aphasia at a network level.

Therefore, in the present study, we used fMRI and dynamic causal modeling (DCM; Friston et al., 2003) to test whether the connectivity of damaged tissue in left hemisphere language regions, their right hemisphere homologues, and remaining ipsilesional domain-general cortex conform to patterns similar to the Heiss and Thiel (2006) hierarchy. Given that lexical-semantic skills are vital to basic language processes such as word comprehension and production, a lexical-semantic network served as a proxy for the entire language network in this study. Specifically, we selected 10 regions of interest (ROIs), including left inferior frontal gyrus, pars triangularis (LIFGtri), angular gyrus (LAG), and middle and inferior temporal gyri (LMTG, LITG, respectively) and their right hemisphere homologues for their hypothesized roles within the canonical language network as well as bilateral middle frontal gyrus (MFG) for its proposed role in domain-general processing (see Table 1).

The first aim of the present study was to determine lexical-semantic network characteristics that best characterize connectivity in healthy older adults versus patients with chronic aphasia. Fig. 1 provides a visual framework of our hypotheses. Within the DCM framework, we created families of network models (see Fig. 1, middle column) to test a chronic aphasia hierarchy similar to Heiss and Thiel (2006). As shown in the top row and middle column of Fig. 1, we hypothesized that controls would demonstrate a preference for left-lateralized connectivity models given that lexical-semantic processing is highly left hemisphere dominant in most healthy individuals (Binder et al., 2009; Price, 2012; Vigneau et al., 2011; Xu et al., 2017). We hypothesized that model fit in PWA would be split between model families—exemplified by other models within the middle column of Fig. 1—given that the model space was constructed to explicitly test whether lesion location dictates effective connectivity in chronic stroke.

Beyond model fit, the DCM framework allows for investigation of the strength and directionality of task-modulated connections between model regions. We predicted that controls would demonstrate stronger connections between the majority of left hemisphere ROIs compared to patients. By contrast, we hypothesized that PWA would rely more heavily on task-modulated connectivity of LMFG than controls given the potential for reorganization to spared extra-sylvian left hemisphere cortex (Meier et al., 2016, 2018; Geranmeyah et al., 2017) and right intrahemispheric connections due to left hemisphere damage.

The second aim was to examine the relationships beween network connectivity, lesion characteristics and language skills in PWA. To expand upon Heiss and Thiel (2006), we hypothesized that neural metrics (i.e., task-based connectivity, left hemisphere damaged tissue) would influence patients' language skills. Specifically, we expected to find

Table 1
Study-specific regions of interest (ROIs) and their proposed functions for language.

Region	Presumed function during language processing	Citations
LMFG	Word retrieval	Price, 2010§
	Domain-general response	Fedorenko et al., 2011, 2012, 2013; Price et al., 2005†
	Executive control of language	Ardila et al., 2016†
LIFGtri	General semantic processing	Friederici and Gierhan, 2013‡; Gabrieli et al., 1998‡; Poldrack et al., 1999†; Vigneau et al., 2006†
	Semantic control	Badre et al., 2005; Friederici and Gierhan, 2013‡; Noonan et al., 2013†; Thompson-Schill et al., 1997; Wagner et al., 2001
	Domain-general cognitive control	Noonan et al., 2013†
	Phonological working memory (dorsal LIFGtri)	Vigneau et al., 2006†
LMTG (all parts)	General semantic processing	Binder et al., 2009
	Phonological/speech processing	Binder et al., 2009
mid LMTG	Lexical-semantic interface	Friederici and Gierhan, 2013‡
LpMTG	Semantic control	Noonan et al., 2013†
	Phonological code retrieval	Indefrey and Levelt, 2000, 2004†
LITG	General semantic processing	Binder et al., 2009†; Price et al., 2005†
	Phonological-semantic interface of visual information	Vigneau et al., 2006†
LAG	General semantic processing	Binder et al., 2009†;
	Semantic control (dorsal LAG)	Noonan et al., 2013†
	Amodal conceptual processing	Vigneau et al., 2006†
	Automatic semantic retrieval (anterior LAG)	Humphreys and Lambon Ralph, 2015†

No marking next to citation indicates single study.
† Indicates meta-analysis.
‡ Indicates review paper.
§ Indicates systematic review. LMFG = left middle frontal gyrus, LIFGtri = left inferior frontal gyrus, pars triangularis, LMTG = left middle temporal gyrus, LITG = left inferior temporal gyrus, LAG = left angular gyrus, p = posterior portion of gyrus.

relationships between lesion location (shown in the left column of Fig. 1), effective connectivity (shown in the middle column of Fig. 1) and language performance (shown in the right column of Fig. 1). We predicted that primary damage to posterior regions would result in functional and structural disconnection of temporoparietal cortex (including LMTG, LAG and/or LITG) and greater reliance on connectivity of intact bilateral anterior structures (as shown in the second model from the top in the middle column of Fig. 1). Primary damage to anterior regions but spared LMFG would result in greater reliance on connections from LMFG to other regions, on connections between left posterior cortex, and on right intrahemispheric interactions (as shown in the third model from the top in the middle column of Fig. 1). Large lesions that affected both anterior and posterior language regions but spared LMFG would result in heavy reliance on LMFG connectivity as well as right intrahemispheric connections (as shown in the fourth model from the top in the middle column of Fig. 1). Finally, we hypothesized that connectivity would be shifted entirely to the right hemisphere in PWA with extensive left hemisphere damage (as shown in the bottom model in the middle column of Fig. 1). As also illustrated in Fig. 1, we hypothesized that less left hemisphere damage (particularly in ROIs) and greater left intrahemispheric connectivity would be related to good lexical-semantic skills and less severe aphasia. By contrast, extensive left hemisphere lesions—particularly lesions extending into LMFG—would result in greater right intrahemispheric and interhemispheric connectivity and poor language abilities.

2. Materials and methods

This work was conducted within the Center for the Neurobiology of Language Recovery (http://cnlr.northwestern.edu/) and is part of a larger project investigating changes in behavioral and neurological metrics following language therapy. Data included in this cross-sectional study were obtained from a pre-treatment phase of the longitudinal study. In addition, a subset of these data has been analyzed and the results reported in previous investigations (Meier et al., 2016, 2018).

2.1. Participants

Thirty-five individuals with chronic aphasia (25 M; mean age: 61.49 ± 10.97 years) and 21 age-matched healthy controls (12 M; mean age: 59.58 ± 13.43 years) were recruited for the study. Patients had a history of a single left hemisphere cerebrovascular accident (CVA) and presented with language deficits as determined by standardized and study-specific behavioral assessments. Contraindications for MR scanning, active medical conditions that prevented participation in study protocols and history of neurological disease (other than stroke in PWA) were not present in participants in either group. All participants exhibited normal or corrected-to-normal vision and hearing and used English as their primary language. Demographic and neurological case history information was collected via questionnaire. Study procedures were conducted in accordance with protocols approved by the Institutional Review Boards of Boston University, Massachusetts General Hospital and Northwestern University and in compliance with the code of ethics per the Declaration of Helsinki.

2.2. Language assessment

A testing battery including standardized and non-standardized assessments was used to measure patients' language deficits. The Western Aphasia Battery-Revised (WAB-R; Kertesz, 2006) was administered to capture patients' overall aphasia severity, as measured by subtests of auditory comprehension and verbal expression that comprise the Aphasia Quotient (AQ). Nonverbal semantic association skills were assessed via the three-picture version of the Pyramids and Palm Trees Test (PPT; Howard and Patterson, 1992). Subtest 51: Word Semantic Association from the Psycholinguistic Assessments of Language Processing in Aphasia (PALPA; Kay et al., 1992) and three non-standardized semantic tasks developed in our laboratory (Meier et al., 2016b) were utilized to assess lexical-semantic skills. Given that lexical-semantic impairments often manifest in word retrieval deficits, naming abilities were assessed with the Boston Naming Test (BNT; Kaplan et al., 2001) and a 180-item non-standardized naming probe. See Table 2 for demographic and testing data for all PWA.

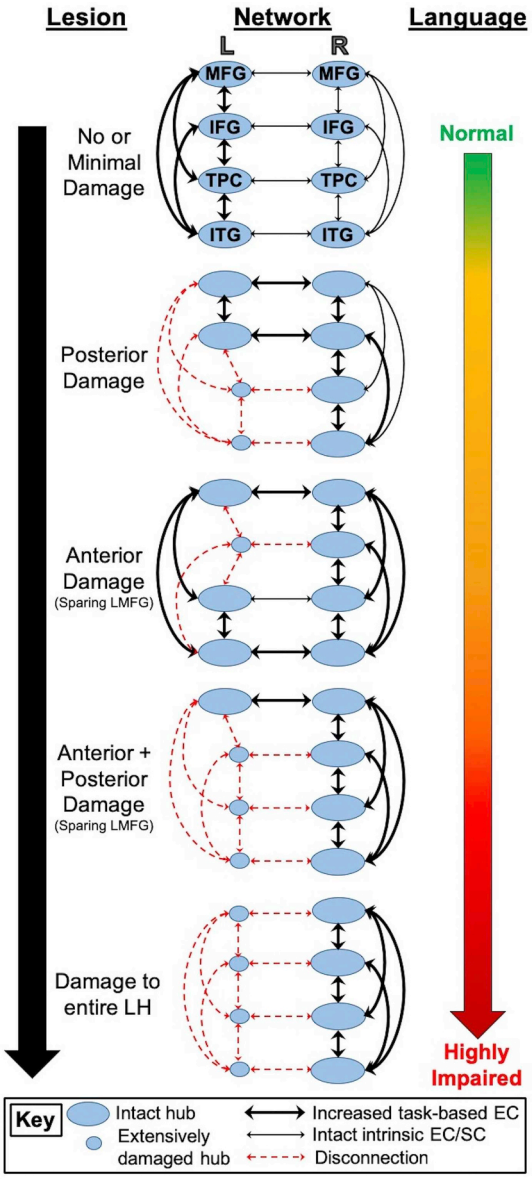

Fig. 1. Hypotheses regarding relationships between lesion location (left column), effective network connectivity (middle column) and language abilities (right column). L/LH = left hemisphere, R = right hemisphere, MFG = middle frontal gyrus, IFG = inferior frontal gyrus, TPC = temporoparietal cortex, ITG = inferior temporal gyrus, EC = effective connectivity, SC = structural connectivity.

2.3. MR data acquisition

MR data were acquired on a 3 T Siemens Trio Tim or Prisma Fit scanner using a 20-channel head + neck coil at the Athinoulous A. Martinos Center in Charlestown, MA or at the Center for Translational Imaging in Chicago, IL between December 2013 and December 2017. High-resolution T1-weighted sagittal images (parameters: TR/TE = 2300/2.91 ms, T1 = 900 ms, flip angle = 9°, matrix = 256 × 256mm, FOV = 256 × 256, slice thickness = 1 mm^3, 176 sagittal slices) and functional images via a gradient echo T2*-weighted EPI sequence (parameters: TR/TE = 2570/30 ms, flip angle = 90°, matrix = 80x78mm, FOV = 220x220mm, 40 axial, 3 mm slices with 2x2x3mm voxels, parallel imaging with acceleration factor or 2) were acquired for all participants.

Each participant completed two runs of an event-related semantic feature judgment task. For each task trial, a picture appeared on the screen, followed one second later by a written feature. In experimental trials (54 items/run), participants saw real pictured objects from three of five semantic categories (i.e., *fruit*, *birds*, *vegetables*, *clothing*, and *furniture*) and were required to make a judgment via button press whether the feature was related or unrelated to the pictured item. Experimental stimuli were balanced for lexical properties (i.e., familiarity, length, frequency, and concreteness) using the CELEX (Van der Wouden, 1990) and MRC Psycholinguistic (Coltheart, 1981) databases. Related semantic features were selected based on results from a MTurk pilot study (https://www.mturk.com/mturk) and classified as either contextual, physical, characteristic or functional in relation to the target item. During control trials (18 items/run), participants saw scrambled, pixelated images in either black/white or color and were required to make a color judgment via button press. Each experimental and control trial was five seconds in duration. A fixation cross appeared on the screen during the inter-stimulus interval, which was jittered to two to four seconds to improve sampling of the hemodynamic response. See Fig. 2A for example trials from the fMRI experiment.

Accuracy and response time (RT) data were collected and compared between groups via Welch's two-sample *t*-tests with unequal variances. Overall, controls had higher accuracy when making real-picture judgments than PWA ($t(40.060) = 5.358$, $p < .001$; controls' mean accuracy: 88.079 ± 4.420%; PWA's mean accuracy: 69.907 ± 18.696%) (Fig. 2B). In contrast, RTs were comparable between groups ($t(46.671) = 1.442$, $p = .156$; controls' mean RT: 1.691 ± 0.194 s; PWA's mean RT: 1.836 ± 0.511 s) (Fig. 2C).

2.4. MR data preprocessing

MR data were preprocessed in SPM12 (http://www.fil.ion.ucl.ac.uk/spm/) using a standard preprocessing pipeline. First, slice timing correction was performed with reference to the middle slice in order to account for timing differences in slice acquisition. Resliced functional images were then coregistered to the T1-weighted structural scan. Next, the T1-weighted image was segmented into white matter, gray matter and cerebrospinal fluid based on SPM12's tissue probability maps and then warped to the ICBM European brain template via affine transformation. Bias-corrected structural and functional images were normalized to MNI space via 4th degree b-spline interpolation. Finally, smoothing of the functional data was performed with a small kernel (i.e., 4 mm) to improve reliability of first-level results but diminish the likelihood of smoothed activations entering lesioned tissue in PWA (Meinzer et al., 2013).

In addition to this standard pipeline, steps were incorporated to ensure the quality of the data. Specifically, for patients, slice-by-slice, manually-drawn lesion maps (with lesioned voxels preserved) and lesion masks (with lesioned voxels deleted) were included in the realignment, coregistration, segmentation and normalization stages to ensure appropriate alignment and masking of the lesion (Brett et al., 2001). For all participants, the alignment of normalized structural and functional images to the template was visually inspected using the Check Reg function in SPM12. Issues with patient T1 alignment to MNI space were mitigated through manual correction of the images or re-running the preprocessing pipeline after skull-stripping. Finally, the Artifact Detection Tools (ART) toolbox (https://www.nitrc.org/projects/artifact_detect/) was used to check for persistent motion artifacts in the normalized functional data. Outlier volumes were identified as those with global signal intensities that deviated > 3 standard deviations from the mean image intensity or volumes that were displaced > 2 mm or rotated > 0.5 rad from the preceding volume.

2.5. Analysis of whole-brain activation

Analysis of the fMRI data was completed to identify ROIs at the group and single-subject level for the effective connectivity analysis. A 1st-level autoregressive general linear model (GLM) that modeled the

Table 2
Demographic, stroke and language testing information in the patient group (AVG = average; SD = standard deviation).

ID	Gender	Age	MPO	Education	Handedness	WAB-R AQ (/100)	PPT (/52)	PALPA 51 (/30)	BNT (/60)	Naming probe (%)	CCJ (%)	CSJ (%)	SFV (%)
P1	M	55	12	16	Right	87.20	50	23	50	58.33	97.50	97.50	93.75
P2	F	50	29	16	Left	25.20	49	3	1	0.99	83.75	81.25	77.50
P3	F	63	62	16	Right	52.00	46	21	10	17.59	85.00	93.75	95.00
P4	M	79	13	16	Right	74.10	49	18	52	67.96	93.75	95.00	90.00
P5	M	67	8	18	Right	30.80	48	9	4	6.11	87.50	77.50	76.25
P6	M	49	113	16	Right	66.60	48	22	44	55.97	91.25	97.50	93.75
P7	M	55	137	16	Right	48.00	46	12	6	14.07	86.25	91.25	88.75
P8	F	71	37	16	Right	95.20	50	26	45	59.07	93.75	100.00	91.25
P9	F	53	12	16	Right	80.40	49	24	37	64.81	98.75	90.00	93.75
P10	M	78	22	18	Right	92.10	49	22	41	33.70	92.50	n/a	91.25
P11	M	68	104	12	Right	40.00	46	12	1	2.78	77.50	72.50	88.75
P12	M	42	18	13.5	Left	92.70	49	21	43	56.94	92.50	96.25	91.25
P13	F	64	24	13	Right	64.40	49	16	41	40.56	100.00	92.50	86.25
P14	F	71	74	12	Right	87.20	44	16	43	56.48	78.75	85.00	90.00
P15	M	61	152	16	Right	74.30	51	21	54	52.22	95.00	100.00	92.50
P16	F	70	152	16	Right	78.00	50	15	24	48.33	100.00	97.50	97.50
P17	M	80	22	18	Right	28.90	43	8	1	7.78	91.25	72.50	85.00
P18	F	48	14	16	Right	13.00	40	10	0	0.00	92.50	77.50	76.25
P19	M	65	16	18	Right	11.70	43	10	0	0.37	81.25	66.25	85.00
P20	M	62	12	16	Right	65.40	37	11	1	7.22	78.75	86.25	88.75
P21	M	60	24	16	Right	45.20	42	6	6	5.19	62.50	62.50	46.25
P22	M	69	170	16	Right	40.40	49	8	3	6.85	93.75	96.25	90.00
P23	F	76	33	18	Right	37.50	34	19	2	2.22	62.50	82.50	20.00
P24	F	64	115	12	Right	58.00	36	12	15	20.56	82.50	88.75	85.00
P25	M	62	15	12	Right	56.00	51	15	21	35.74	87.50	92.50	93.75
P26	M	49	49	12	Right	85.50	49	20	53	68.61	96.25	96.25	95.00
P27	M	81	11	12	Right	73.80	51	22	24	40.56	n/a	n/a	n/a
P28	M	49	67	12	Right	32.30	44	2	3	5.00	82.50	87.50	80.00
P29	M	39	18	16	Right	71.30	52	14	36	47.22	93.75	98.75	97.50
P30	M	64	13	12	Left	79.60	50	17	41	45.93	92.50	97.50	93.75
P31	M	62	21	16	Left	91.50	46	18	42	74.26	95.00	96.25	92.50
P32	M	68	21	13.5	Right	82.50	49	12	33	31.48	91.25	97.50	91.25
P33	M	58	23	14	Right	61.80	51	18	10	11.94	92.50	93.75	93.75
P34	M	53	467	17	Right	94.00	50	26	55	65.74	93.75	92.50	95.00
P35	M	47	19	16	Right/ambi	91.40	47	24	55	66.67	93.75	96.25	n/a
AVG		61.49	59.97	15.11		63.09	46.77	15.80	25.63	33.69	88.75	89.36	86.25
SD		10.97	85.50	2.08		24.73	4.50	6.43	20.54	25.42	9.03	10.06	15.17

MPO = months post-onset; WAB-R AQ = Western Aphasia Battery-Revised Aphasia Quotient; PPT = Pyramids and Palm Trees Test; PALPA = Psycholinguistic Assessments of Language Processing in Aphasia; BNT = Boston Naming Test; CCJ = Category Coordinate Judgment; CSJ = Category Superordinate Judgment; SFV = Semantic Feature Verification; ambi = ambidextrous.

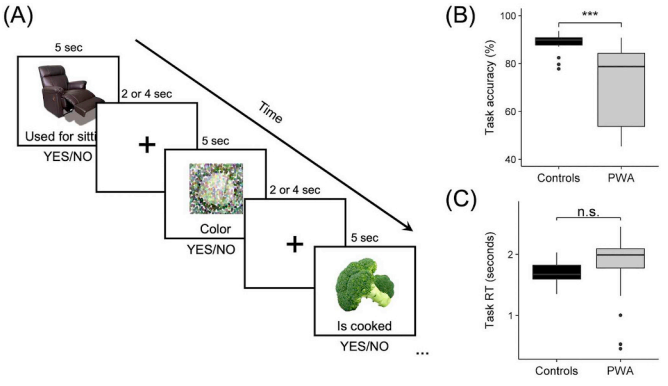

Fig. 2. fMRI task. (A) Example time series of experimental trials of real pictured items and scrambled control trials with 2–4 s inter-stimulation intervals. Differences between groups in fMRI task (B) accuracy and (C) response time (RT). *** $p < .001$, n.s. = not significant.

canonical hemodynamic response function plus its temporal derivative was used for all participants. The GLM included concatenated data from each run of the fMRI task. Experimental (i.e., *PICS*), control (i.e., *SCR*) and fixation (i.e., *FIX*) conditions were modeled as effects of interest, and motion parameters and outlier volumes from each run were included as nuisance regressors. For the purpose of the connectivity analysis, 1st-level activation maps of the contrast of interest *PICS – SCR* were obtained at an uncorrected threshold ($p < .001$). In the event that activation was not observed within ROIs at the single-subject level at this threshold, the procedure outlined in the section 2.6.2. entitled "Localization of volumes of interest" was followed.

Second-level analyses of the *PICS – SCR* contrast were performed to identify regions of robust whole-brain activation. Given the heterogeneity of lesion location and behavioral profiles of our patient sample, a voxel-wise uncorrected threshold of $p < .001$ was used to identify distinct activation peaks within ROIs for each group. Of the 10 ROIs selected a priori based on the literature, only ROIs active at the 2nd level in patients and/or controls were included in the effective connectivity analysis. To confirm that activation extracted at the uncorrected threshold was characteristic of activity within each group, multi-subject one-sample *t*-tests with a cluster-defining uncorrected threshold of $p < .01$ and F.W.E. cluster-corrected threshold of $p < .05$ were conducted with 10,000 permutations using the Statistical non-parametric mapping (SnPM) toolbox (http://warwick.ac.uk/snpm).

2.6. Effective connectivity analysis

Dynamic causal modeling (DCM; Friston et al., 2003; Kahan and Foltynie, 2013; Stephan et al., 2010, 2017) is a method of task-based effective connectivity that uses Bayesian estimations on causal interactions between modeled regions to make inferences regarding how changes in activity in one region affect the rate of change in another region and how interregional coupling is affected by external task conditions. The biophysical properties of neuronal activity and hemodynamic responses to external stimuli are modeled within five state

equations in the DCM framework. Four of these equations comprise a hemodynamic forward balloon model that models changes in activity-dependent signals and subsequent changes in blood flow and volume and in deoxyhemoglobin. The fifth and final state equation captures the dynamics of neuronal activity through three parameters, modeled via matrices. The DCM-A matrix measures the latent connectivity of modeled regions in the absence of task inputs. The DCM-B matrix reflects the effect of external task conditions on the connectivity between modeled regions. Finally, the DCM-C matrix captures exogenous input of task effects on regions within the model.

Crucially, DCM is used to test specific, biologically-plausible hypotheses about subnetworks of regions (as opposed to other connectivity approaches that aim to delineate an entire network). As such, the three parameters within the neuronal state equation were specified according to known evidence regarding neurobiology and to test biologically plausible models of neural reorganization of language in chronic aphasia (as schematized in Fig. 1). First, all possible intrahemispheric connections and connections between homologous interhemispheric regions were specified in the DCM-A matrix. Across models, the exogenous task effect of *PICS* was modeled either to LITG, RITG or bilateral ITG given the nature of the semantic task and literature implicating inferior temporal cortex in early conceptual processing of visually presented material (Binder et al., 2009). The DCM-B matrix was specifically structured to mimic the hypothesized task-based connectivity patterns of the lesion groups illustrated in Fig. 1. Specifically, the model space contained 14 individual models, partitioned into four model families. Of the 10 ROIs identified in Table 1, only regions activated at a second level in patients and/or controls were included in the model space. Note that the models shown in Fig. 1 are included in the model space but alternative models were also constructed (see section 2.6.1 below).

2.6.1. Model specification

2.6.1.1. Family A: Left-lateralized connectivity (i.e., no/minimal damage). These models represented plausible semantic network connectivity in healthy, older adults. Specifically, model #1 included bidirectional connections between all left hemisphere regions and represented the extreme case of left-lateralized connectivity. This model mirrors the first model from the top in Fig. 1. Model #2 was similar to model #1 with the exception that task input to bilateral ITG and bidirectional interhemispheric connections between LITG and RITG were specified to reflect the likelihood of bilaterally represented low-level semantic processing. Models #3 and #4 mirrored models #1 and #2, respectively, with the addition of bidirectional connections between interhemispheric prefrontal regions. These models were created to align with the literature citing a reduction in hemispheric asymmetry of prefrontal cortex as a function of normal aging (Cabeza, 2002).

2.6.1.2. Family B: Bilateral anterior-weighed connectivity (i.e., posterior damage models). The three models in this family were specified to reflect potential neural reorganization following damage to left posterior regions implicated in semantic processing (e.g., LMTG, LAG) due to middle cerebral artery (MCA) infarct. Model #5 was created under the assumption that the likelihood of extensive damage to LITG in the patient group would be low given the vascular distribution of the MCA. As such, bidirectional connections were specified between left prefrontal regions and LITG in this model. Greater task modulation of bilateral anterior connections as well as posterior right hemisphere regions were also specified in model #5 as a likely outcome of left temporoparietal damage. Model #6 mirrored model #5 but represented network connectivity in the event of intact local recruitment of LITG but functional disconnect of LITG from other left hemisphere regions due to lesion. Model #7 was specified to model the potential ramifications of extensive damage to all temporoparietal cortex, including LITG. A similar model is visualized in the second model from the top in the middle column of Fig. 1.

2.6.1.3. Family C: Bilateral posterior-weighted connectivity (i.e., anterior damage models). Models within this family were designed to reflect potential functional reorganization in the event of damage to left inferior frontal regions with sparing of dorsolateral prefrontal cortex. Model #8 modeled connections between left dorsolateral prefrontal cortex and left posterior regions as well as bidirectional right intrahemispheric connections and connections between left dorsolateral prefrontal and right prefrontal cortices. Model #9 was the same as model #8 with the addition of exogenous task input to RITG and bidirectional connections between bilateral ITG. Model #10 mirrored model #9 with additional bidirectional connections between RIFGtri and RITG as potential right hemisphere compensation for lost LIFGtri connections. A similar model is visualized in the third model from the top in the middle column of Fig. 1.

2.6.1.4. Family D: Right-lateralized connectivity (i.e., extensive left hemisphere damage). Models within this family were created to reflect potential connectivity patterns in the event of damage to anterior and posterior "classic" language cortex (i.e., models #11–13) and extensive left hemisphere damage not only to traditional language regions but extending into dorsolateral prefrontal cortex (i.e., model #14). Similar to previously-described models, model #11 was created to reflect potentially-intact connections including inferior temporal and dorsal prefrontal regions, which would be least likely to be damaged after MCA stroke. Model #12 was created with the assumption that left inferior temporal and dorsal prefrontal regions may remain functionally connected to right hemispheric homologous regions even in the event of left intrahemispheric disconnect. Similarly, model #13 mirrored model #12 with the exception of exogenous task input and connectivity of LITG. Finally, model #14 was created to illustrate the most extreme case of right-lateralized task-based connectivity in the event of extensive damage to the entire left hemisphere. Models #13 and #14 mirrored the last two models shown in the middle column of Fig. 1.

Following construction of the DCM model space, volumes of interest (VOIs) were identified for each participant (see below) and the models were specified and estimated for each subject. Bilinear, two-state and non-stochastic modeling (Marreiros et al., 2008; Seghier et al., 2010) was implemented using the DCM10 toolbox within SPM12.

2.6.2. Localization of volumes of interest

Procedures similar to those utilized in Meier et al. (2018) were used to ensure activity was extracted from a similar anatomical location within each ROI across participants. Regions that were active at the 2nd level in patients and/or controls were included in the final model space. The 2nd-level peak maxima served as the center point of 35x50x35mm (or in the case of bilateral IFGtri, 30x30x30mm) bounding boxes created using MarsBaR (Brett et al., 2002). If a region was activated in both groups at the 2nd level, homotopic bounding boxes were created for each group and combined. Bounding boxes were subsequently trimmed to fit the anatomical boundaries of ROIs per the Automated Anatomical Labeling (AAL) atlas (Tzourio-Mazoyer et al., 2002). Next, left hemisphere anatomically-constrained bounding masks were lesioned by intersecting each patient's manually-drawn lesion map with the masks and by retaining only non-lesioned mask voxels. The amount of spared tissue within each lesioned mask was calculated so that the potential functionality of remaining tissue could be assessed for each patient and ROI. Last, 1st-level peak maxima for *PICS – SCR* within each ROI were identified for each participant.

The MNI coordinates corresponding to these peaks served as the center of VOIs in the form of 8 mm eigenvariate spheres of the task time series. In the event that activity at the prescribed threshold (i.e., $p < .001$, uncorrected) was not observed within a given region for an individual, the threshold was lowered to $p < .01$. If activation was still not observed, a three-tiered decision process was implemented. First, if

the subject was a patient who did not exhibit activation within a highly-damaged left hemisphere region (i.e., < approximately 50% spared tissue within the regional bounding mask), a noisy signal (at $p = 1.0$, uncorrected) was extracted at the group-level MNI coordinate for that region. Noisy VOIs have been used in previous DCM studies of stroke patients (Meier et al., 2018; Seghier et al., 2012, 2014) as they represent a good approximation of damage to a region due to lesion (Seghier et al., 2010) and allow for the inclusion of patients who would otherwise be excluded from the analysis due to incompatible DCM matrices. Second, if a participant in either group did not exhibit activation within a region outside the "classic" language network (i.e., left dorsolateral prefrontal cortex, any right hemisphere ROI), a noisy signal was similarly extracted. The rationale here was to allow for comparison between participants (e.g., healthy controls, patients with minimal left hemisphere damage) who may require only left hemisphere language cortex for lexical-semantic processing to subjects who activate additional regions (e.g., patients with a high degree of left hemisphere damage). If neither of these scenarios applied and a participant did not exhibit activity, then that participant was excluded from the DCM analysis.

2.6.3. Model-level inference

Following VOI localization and model estimation, inferences regarding the DCM results were made at the model level. First, Bayesian parameter averaging (BPA; Stephan et al., 2010) was performed across outputs from the two runs of the task so that one set of models for each participant remained. A random effects Bayesian model selection (BMS; Penny et al., 2004) was performed at the individual and group levels to determine which of the 14 models exhibited the highest probability of explaining semantic network connectivity beyond prior expectation. Given potential uncertainty in the model structure (especially within model families), a family-wise BMS (Penny et al., 2010) was also performed for each participant and each group to determine which family of models best fit the data. Within the family-wise BMS analysis, Bayesian model averaging (BMA) was performed such that averages were weighted according to model fit across all families and models.

2.6.4. Parameter-level inference

Following model-level inference, inferences on task-modulated parameters (within the DCM-B matrix) were made. Within the DCM framework, task-modulated connections (measured via Ep.B values, in Hertz) reflect regions that are functionally in-sync during the experiment. Specifically, change in activity due to external task effects in the driving region of a connection (e.g., LIFGtri in LIFGtri➔LITG and LIFGtri➔RIFGtri) results in a change in activity in the target region (e.g., LITG and RIFGtri in LIFGtri➔LITG and LIFGtri➔RIFGtri). Within the two-state DCM framework implemented in the present study, Ep.B values capture not only the strength of the connection but also the directionality of the effect. Positive Ep.B values are typically interpreted as excitatory (where the change in activity in a driving region increases the activity within the target region) whereas negative values are interpreted as inhibitory. An Ep.B value of 0 indicates null recruitment of a connection.

To address aim 1 and determine the connections most critical for PWA and controls, one-sample *t*-tests were conducted on coupling parameters (i.e., Ep.B values) within each group, corrected at a false discovery rate (FDR; Benjamini and Hochberg, 1995) at $p < .05$ for multiple tests (i.e., 24 tests, one per connection). Next, between-group differences in task-modulated connections were examined via three one-way MANOVA models in which the independent variable in each model was group (PWA vs. controls) and the dependent variables were Ep.B values from either the 12 left intrahemispheric connections (MANOVA #1), six right intrahemispheric connections (MANOVA #2) or six interhemispheric connections (MANOVA #3). FDR correction was applied first on the *p*-values from the three multivariate models, followed by correction for each univariate test within each model.

2.7. Relationships between effective connectivity, lesion characteristics and behavior in PWA

To address aim 2, we conducted two sets of analyses within patients to investigate relationships between task-based effective connectivity (per DCM task-modulated connection parameters), lesion characteristics (per percent damage to regions implicated in lexical-semantic processing and total lesion volume) and language abilities (per fMRI task accuracy, fMRI task RTs and WAB-R AQ).

2.7.1. Relationship between effective connections and lesion factors

First, we conducted two principal component analyses (PCAs) on patient data to reduce connectivity and lesion variables into a smaller, more manageable set of factors. One PCA included all 24 task-modulated connection parameters (i.e., 12 left intrahemispheric, six right intrahemispheric connections and six interhemispheric connections) from the DCM analysis. The second PCA included lesion data from an expanded set of 20 ROIs that mapped onto the regions and connections illustrated in Fig. 1. In addition to cortical regions explicitly included in the DCM analysis (i.e., LMFG, LIFGtri, LMTG, LAG and LITG), the expanded ROI set included intrahemispheric white matter association pathways (i.e., left arcuate fasciculus [LAF], including anterior, posterior and long segments; left inferior longitudinal fasciculus [LIFOF], left inferior longitudinal fasciculus [LILF], left uncinate fasciculus [LUF]) and commissural tracts (i.e., left corpus callosum [LCCallosum] and left anterior commissure [LaCommissure]) that have been implicated in language processing (e.g., Binney et al., 2012; Catani and Mesulam, 2008; Catani et al., 2002; Catani et al., 2005; Cloutman and Lambon Ralph, 2012; Frey et al., 2008; Glasser and Rilling, 2008; Parker et al., 2005; Sarubbo et al., 2013; Saur et al., 2008; Turken and Dronkers, 2011) and either directly or indirectly connect DCM ROIs. Cortical ROIs that additionally serve as the end points of the aforementioned association pathways[1] were also considered, including left precentral gyrus (LPreCG), inferior frontal gyrus, pars opercularis (LIFGop), supramarginal gyrus (LSMG) and superior temporal gyrus (LSTG) for connecting LAF segments and LIFG, pars orbitalis (LIFGorb) and the anterior temporal pole—split into superior [LSTGpole] and middle [LMTGpole] segments—as the end points of the LUF. The percentage of damaged tissue in these 12 cortical and 8 white matter ROIs was extracted from an atlas that combined the AAL atlas with Catani and Thiebaut de Schotten's (2008) white matter tractography atlas within NiiStat (https://github.com/neurolabusc/NiiStat) and entered into the lesion PCA.

A varimax rotation was applied to each PCA. The number of components retained was determined by visual inspection of scree plots and confirmed by parallel analyses run in the 'paran' package in R (Dinno, 2012). To characterize components, variable loadings of ≤ -0.50 or ≥ 0.50 were used to determine which DCM parameters or lesion variables loaded most heavily onto each component. Single-subject weighted scores were then extracted and used in subsequent analyses. To examine links between DCM connectivity parameters and lesion characteristics, backward stepwise regression models were used to predict each DCM connection component from lesion variables (i.e., lesion components and total lesion volume). Model assumptions were checked using the 'car' (Fox and Weisburg, 2011), 'MASS' (Venables and Ripley, 2002) and 'gvlma' (Pena and Slate, 2014) packages in R.

Follow-up analyses were run to determine whether the usage of noisy VOIs influenced the relationships between DCM and lesion components. First, we identified regions from which noisy VOIs were extracted for more than one patient. Next, we conducted Spearman

[1] The inferior and middle occipital gyri serve as the posterior termination of the ILF and IFOF; however, these ROIs were excluded from the lesion analysis because they were relatively intact within the patient sample and are implicated in visual, not language, processes.

correlations between each DCM component and binary noisy VOI variables (reflecting the presence/absence of an extracted noisy signal). Finally, if noisy VOIs were significantly associated with DCM component connectivity ($p < .05$, uncorrected), the noisy VOI variable was added to the corresponding aforedescribed regression model to determine if relationships between DCM and lesion components persisted when controlling for noisy VOIs.

2.7.2. Effective connectivity and lesion predictors of language skills

To examine the relationship between connectivity, lesion and language, the DCM connection and lesion components previously described in section 2.7.1. were used as independent predictors of language variables in another series of backward stepwise regression models. Separate models were run for each dependent variable, including a measure of lexical-semantic knowledge (i.e., fMRI task accuracy), a measure of lexical-semantic processing speed (i.e., fMRI task RT) and a measure of overall aphasia severity (i.e., WAB-R AQ). Of note, exponentiated RT (i.e., RT^{exp}) was used rather than raw RT in order to correct for the left skew of the raw data and to improve the distribution of the residuals in reaction time models. Model assumptions were again checked using the aforementioned packages.

3. Results

3.1. Whole-brain activity

Within the original sample, MR data were unusable due to hardware issues for two controls and due to artifact from implanted material in one patient (P35). Imaging data were not collected for another control subject due to claustrophobia in the scanner. Ultimately, fMRI data from 18 controls and 34 PWA were included in analyses of brain activation.

To characterize whole-brain activity and identify peaks within ROIs selected a priori, 2nd-level activation maps for *PICS-SCR* at an uncorrected voxel-wise threshold ($p < .001$) were obtained (see the left panel of Fig. 4). In controls, the largest cluster was located in left posterior temporo-occipital cortex with sub-peaks located in LITG and the left fusiform gyrus. Another large posterior cluster was localized in the right middle and inferior occipital gyri and right fusiform gyrus with extension into right middle and inferior temporal gyri. Peak frontal activity in controls was found in all three parts of LIFG as well as clusters in left supplementary motor area (LSMA) and left superior medial frontal gyrus. In PWA, like controls, the largest clusters of activity were found in posterior regions, including bilateral ITG with extension into neighboring inferior occipital and fusiform gyri. Smaller posterior clusters were found in LAG, LMTG and left lingual gyrus. Peak frontal activity was located in LSMA with extension into superior and middle dorsomedial and dorsolateral prefrontal cortex. Another cluster was found in ventral frontal regions, with sub-peaks within LIFG, pars orbitalis, left precentral gyrus and left posterior orbitofrontal cortex. These patterns of activation are consistent with the permutation test results (see Supplementary Material, Fig. S1).

Activation peaks were found in eight of the original 10 ROIs (no RAG or RMFG peaks) in controls and/or patients at the group level. It should be noted that the cluster PWA activated in the left temporoparietal cortex had sub-peaks in LMTG and LAG. Therefore, these two ROIs were collapsed into a single left temporoparietal cortex (LTPC) ROI. Thus, the final DCM model space (shown in Fig. 3) included seven ROIs.[2] The MNI coordinates corresponding to regional peaks within each group (see Fig. 4) were used to create bounding masks to constrain the search space for extraction of individual participant peaks used in the effective connectivity analysis.

3.2. Tissue integrity and activation within cortical masks

Bounding masks created based on the 2nd-level analyses are shown in Supplementary Material, Fig. S2. The lesioned tissue calculations revealed that the LIFGtri and LTPC masks were the most damaged regions across the patient group whereas the most spared left hemisphere ROI was LITG followed by LMFG (see Table 3). These findings are consistent with the whole brain lesion overlay (Fig. 5), which shows that the greatest areas of left hemisphere damage were localized to frontal and temporal lobe tissue nearest the Sylvian fissure.

For the effective connectivity analysis, noisy VOIs were extracted from LIFGtri for eight PWA (P5, P11, P18, P21, P22, P32, P33 and P34), LTPC for another eight PWA (P1, P4, P5, P6, P9, P25, P27 and P28), LMFG for two PWA (P21 and P28) and LITG for one patient (P20) due to anatomical damage. As per the previously-described VOI localization decision procedure, noisy VOIs were also extracted from ROIs outside the LIFGtri-LTPC-LITG lexical-semantic subnetwork, including LMFG for one patient (P13), RIFGtri for six patients (P4, P8, P11, P18, P25 and P30) and RMTG for one patient (P27) and one control. Four patients (P3, P10, P19 and P29) and one control demonstrated minimal activity within the majority of ROI masks and were excluded from the DCM analysis. All participants included in the effective connectivity analysis (i.e., 30 PWA and 17 controls) had at least five functional VOIs. VOI overlays for all controls and all PWA are shown in Supplementary Material, Figs. S3A and S3B, respectively. For each ROI, the distance between participants' peak maxima and the center of ROI masks was calculated using the formula $d = \sqrt{(x_2 - x_1)^2 + (y_2 - y_1)^2 + (z_2 - z_1)^2}$. No significant between-group differences were found in distance metrics for any ROI (LMFG: $t(42) = -0.349$, $p = .729$; LIFGtri:$t(37) = -0.955$, $p = .345$; LTPC: $t(37) = -0.171$, $p = .865$; LITG:, $t(44) = -0.599$, $p = .552$; RIFGtri: $t(39) = 1.009$, $p = .319$; RMTG: $t(43) = 1.235$, $p = .228$; RITG: $t(45) = 0.370$, $p = .713$), indicating that activation used in the DCM analysis was extracted from a similar location within MNI space and was comparable in patients and controls across regions (see Supplementary Material, Fig. S3C).

3.3. DCM model-level inference

Single-subject and group-level model fit was quantified by the exceedance probability (xp) values of each model and model family. High xp values (e.g., ≥ 0.90) reflect that a given model or family explains the variance in the time series to a greater extent than prior expectation suggests. Consistent with our hypotheses, Family A: Left-lateralized connectivity (i.e., no/minimal damage) was a good fit for controls' data with an xp value of 0.949. The best-fit individual model was model #4 (xp = 0.750) followed by model #2 (xp = 0.151) in the control group. Contrary to our hypotheses, the best-fit families in PWA were Family A: Left-lateralized connectivity (i.e., no/minimal damage) (xp = 0.568) and Family C: Bilateral posterior-weighted connectivity (i.e., anterior damage models) (xp = 0.424). Nonetheless, consistent with the family-wise BMS findings, the best-fit individual model was model #10 (xp = 0.527) followed by models #4 (xp = 0.3341) and #2 (xp = 0.054) in the patient group. See Fig. 6 for a visualization of the model fit results. As mentioned previously, because of the heterogeneity in model fit, BMA weighted across all model families was performed, which yielded a single set of parameters for each participant that was further examined.

[2] Since the whole-brain activation results dictated the final regions included within the model space, the regions shown in Figures 1 and 3 differ. Specifically, while we hypothesized that RMFG would be activated by the fMRI task (as in Figure 1), no activity within this region was found, and thus, it was excluded from the model space (see Figure 3). Activity was found in RMTG, not RAG; therefore, the region labeled RTPC in Figure 1 was relabeled RMTG in Figure 3.

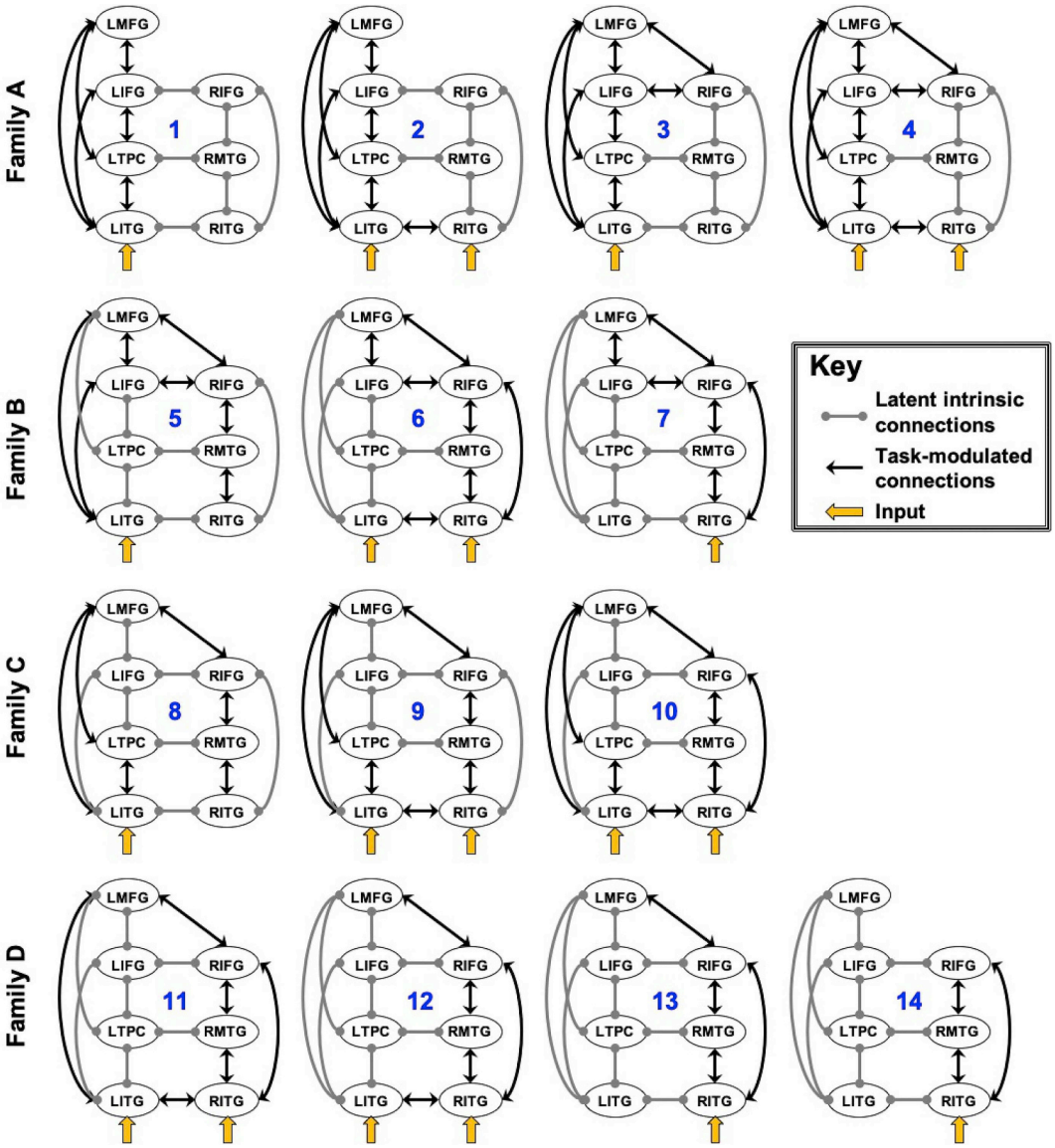

Fig. 3. DCM model space. Fourteen individual models (#1–14) were constructed that belong to one of four model families, including Family A: Left-lateralized connectivity (i.e., no/minimal damage), Family B: Bilateral anterior-weighted connectivity (i.e., posterior damage models), Family C: Bilateral posterior-weighted connectivity (i.e., anterior damage models) and Family D: Right-lateralized connectivity (i.e., extensive left hemisphere damage). Latent connections (denoted by gray lines) were specified between all intrahemispheric ROIs and between interhemispheric homologues. The direction of task-modulated connections (denoted by the arrowhead) varied from model to model and was specified according to hypotheses regarding network connectivity patterns in healthy individuals and PWA. Task input (indicated by thick yellow arrows) was modeled to LITG and/or RITG in each model.

3.4. DCM parameter-level inference

One-sample *t*-tests of controls' task-modulated connections for *PICS* yielded significant results only for connections driven by LITG (i.e., LITG➔LIFGtri, LITG➔LMFG, LITG➔LTPC, and LITG➔RITG) (Fig. 7A). On the other hand, the semantic condition of *PICS* significantly modulated many bilateral connections within the patients' semantic network. Like controls, the LITG-driven connections were significant, and additional significant connections included LIFGtri➔LMFG within the left hemisphere, interhemispheric connections (i.e., LIFGtri➔RIFGtri and RITG➔LITG) and several right intrahemispheric connections (i.e., RIFGtri➔RMTG, RITG➔RIFGtri and RITG➔RMTG) (Fig. 7B).

When comparing the two groups directly with one-way MANOVAs, the overall effect of group was not significant for right intrahemispheric task-modulated coupling ($F(6,40) = 0.771$, Pillai's trace = 0.104, unadjusted $p = .597$, FDR-adjusted p = .597). The main effect of group was on the cusp of significance for interhemispheric connectivity ($F(6,40) = 2.337$, Pillai's trace = 0.260, unadjusted $p = .050$, FDR-adjusted $p = .075$), yet none of the univariate effects of the interhemispheric model survived multiple comparison correction. By contrast, the effect of group was significant in the left intrahemispheric connection model ($F(12,34) = 3.518$, Pillai's trace = 0.554, unadjusted $p = .002$, FDR-adjusted p-value = .006). After FDR correction, univariate results showed that modulation by the semantic task resulted in stronger excitatory coupling for LITG➔LIFGtri ($F(1,45) = 18.826$, $p = .001$) and LITG➔LTPC ($F(1,45) = 9.393$, $p = .022$) in controls relative to PWA. Of note, the between-group differences were the result of differences in connection strength rather than the nature of the connections. Specifically, excitatory, rather than inhibitory, task-modulated coupling was found for all connections significantly recruited within each group. Complete between-group multivariate and univariate results are shown in Table 4.

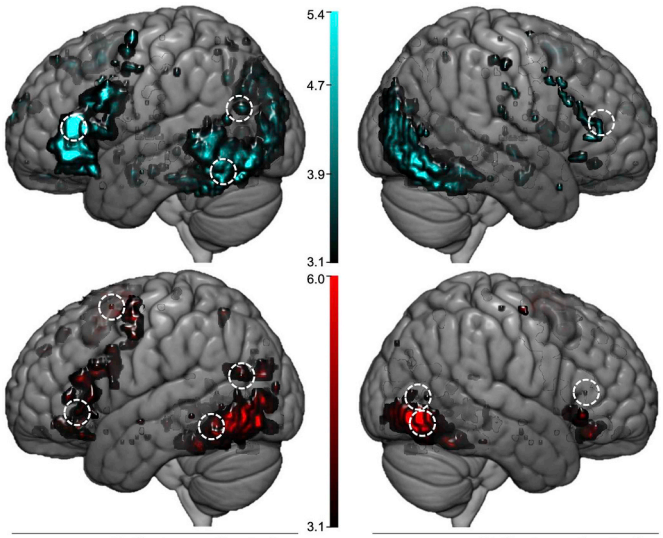

Region	Patients (in red)	Controls (in cyan)
LMFG	-33 9 60	n/a
LIFGtri	-42 30 -3	-45 30 9
LTPC	-42 -69 18	-48 -69 21
LITG	-48 -51 -12	-51 -60 -18

Region	Patients (in red)	Controls (in cyan)
RIFGtri	42 30 9	54 39 12
RMTG	51 -72 6	[39 -87 12]
RITG	45 -69 -9	[42 -84 -3]

Fig. 4. Whole brain activation in controls (in cyan, at top) and patients (in red, at bottom) at an uncorrected threshold ($p < .001$). Peak maxima within each ROI within each participant group are denoted by dashed-lined circles with MNI coordinates corresponding to each peak listed in the tables at the bottom of the figure. In controls, peak maxima for clusters of activation in RMTG and RITG were found in middle and inferior occipital cortex, respectively; MNI coordinates for these peaks are shown in brackets.

3.5. Relationships between lesion characteristics, effective connectivity and language skills in PWA

The PCA of task-modulated connections resulted in a total of five components that explained 66% of the variance in Ep.B values. As shown in Fig. 8A, four right intrahemispheric connections (i.e., RIFGtri➔RITG, RIFGtri➔RMTG, RMTG➔RIFGtri and RMTG➔RITG) and one interhemispheric connection (i.e., LIFGtri➔RIFGtri) positively loaded onto the first connectivity component, hereafter referred to as CC1: RH connectivity. The second component included positive loading of three connections with modulated bilateral frontal regions (i.e., LIFGtri➔LMFG, RIFGtri➔LIFGtri and RITG➔RIFGtri) and negative loading of LITG➔LTPC; given the positive loadings, this component was dubbed CC2: Target bilateral frontal ROIs. The third component—renamed CC3: IntraLH, target frontal ROIs—included positive loadings of left intrahemispheric connections (i.e., LITG➔LIFGtri, LMFG➔LIFGtri, LTPC➔LIFGtri, LTPC➔LMFG) in which left frontal regions were modulated by other left hemisphere ROIs. The three connections in which LITG was modulated by other left hemisphere regions (i.e., LIFGtri➔LITG, LMFG➔LITG and LTPC➔LITG) positively loaded onto the fourth component—renamed CC4: IntraLH, target LITG. Last, a mix of positive (i.e., LIFGtri➔LTPC and LMFG➔LTPC) and negative (i.e., LITG➔RITG, RITG➔LITG) loadings comprised the fifth component—dubbed CC5: Target bilateral posterior ROIs. Certain connections did not load heavily onto any component; nonetheless, this five-component solution was retained to minimize the number of DCM variables in subsequent analyses.

The PCA of lesion variables loaded onto five principal components that explained approximately 83% of the variance in damaged tissue data.[3] As shown in Fig. 8B, the first lesion component—renamed LC1: Dorsal damage—included heavy positive loading of frontal dorsal structures (i.e., LPreCG, LMFG, all parts of LIFG, LSMG and LAF anterior and long segments) and LUF and LSTG, structures anteriorly connected to dorsal regions. Temporal lobe regions and tracts (i.e., LSTG, LSTGpole, LMTG, LMTGpole, LITG, LILF and the posterior segment of LAF) positively loaded onto the second component, renamed LC2: Ventral damage. Structures that positively loaded onto the third component—dubbed LC3: Parietal damage—included LSMG, LAG and the posterior portion of the LAF. Positive loadings of LPreCG, LMFG and LCCallosum comprised the fourth component, renamed LC4: Superior frontal damage. The final component—renamed LC5: WM

Table 3
Lesion volume and percentage of spared tissue in each DCM ROI mask in PWA (AVG = average; SD = standard deviation).

ID	Lesion volume	LMFG	LIFGtri	LTPC	LITG
P1	57,246.00	100.00	100.00	42.59	100.00
P2	249,934.00	91.96	30.50	89.24	96.12
P3	175,378.00	100.00	99.94	1.77	92.62
P4	84,778.00	100.00	100.00	32.50	92.09
P5	171,944.00	100.00	79.38	30.90	90.33
P6	298,967.00	75.93	9.66	2.68	97.87
P7	181,973.00	97.05	93.21	61.07	99.99
P8	11,660.00	100.00	100.00	100.00	100.00
P9	76,553.00	100.00	100.00	44.28	100.00
P10	32,114.00	100.00	100.00	99.99	80.58
P11	186,845.00	99.36	19.58	89.06	99.99
P12	12,131.00	100.00	99.85	99.53	100.00
P13	96,932.00	94.64	60.82	87.06	100.00
P14	189,309.00	59.08	87.23	84.16	100.00
P15	163,488.00	99.98	52.03	68.77	99.89
P16	69,643.00	99.82	92.39	99.32	100.00
P17	89,026.00	99.79	61.69	95.54	100.00
P18	164,327.00	100.00	11.98	73.29	100.00
P19	247,593.00	79.34	9.00	69.40	99.99
P20	100,019.00	100.00	100.00	99.19	52.92
P21	172,812.00	11.63	67.49	90.84	100.00
P22	183,449.00	99.03	60.89	26.01	99.72
P23	184,390.00	95.32	84.67	75.49	96.99
P24	127,704.00	79.39	72.82	88.55	99.72
P25	76,654.00	100.00	88.29	64.51	100.00
P26	87,587.00	100.00	92.44	99.99	99.97
P27	51,699.00	100.00	100.00	54.11	96.89
P28	317,071.00	2.00	53.92	30.07	89.24
P29	26,221.00	100.00	99.52	97.94	100.00
P30	34,148.00	100.00	96.49	100.00	100.00
P31	1565.00	100.00	100.00	100.00	100.00
P32	80,283.00	90.52	3.14	100.00	100.00
P33	186,520.00	62.29	12.99	100.00	100.00
P34	120,817.00	95.25	39.96	94.12	99.97
AVG	126,787.65	89.19	70.00	73.29	96.61
SD	82,129.98	23.49	33.63	30.15	8.82

Notes: Lesion volume in mm^3. Percentage of spared tissue in each cortical mask, including left middle frontal gyrus (LMFG), left inferior frontal gyrus, pars triangularis (LIFGtri), left temporoparietal cortex (LTPC) and left inferior frontal gyrus (LITG).

[3] For the lesion PCA, parallel analysis suggested retention of two components (*footnote continued*) that explained approximately 59% of variance in the data. These components aligned with the bifurcation of the middle cerebral artery: dorsal structures loaded onto the first component whereas ventral structures loaded onto the second component (see Supplemental Figure 4). While the two-component solution is reasonable from an anatomical perspective, the coarseness of this parcellation prohibited testing the nuanced relationships between lesion and other factors outlined in the study aims. Moreover, neither LAG or LITG—two regions within the DCM analyses—heavily loaded onto either component. Thus, we utilized an alternative criterion of retaining components with eigenvalues > 1.0 (Kaiser, 1960; Kaiser and Caffrey, 1965), resulting in the five-component solution. Note, however, that all subsequent analyses were replicated with the two-component lesion PCA solution; the results are reported in Supplementary Material Tables S1 and S2.

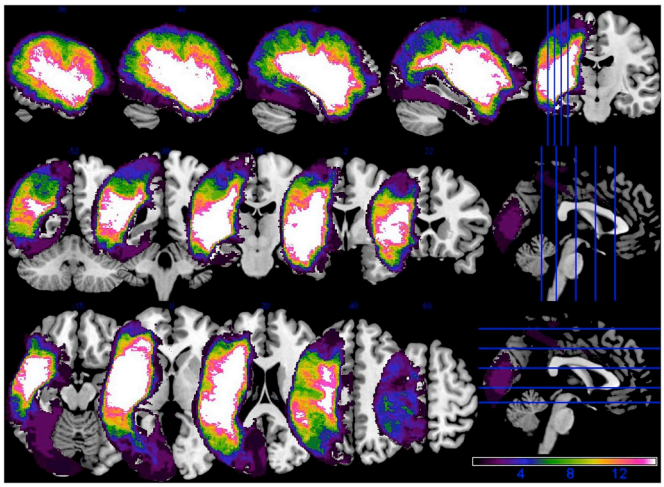

Fig. 5. Overlay of patients' lesions.

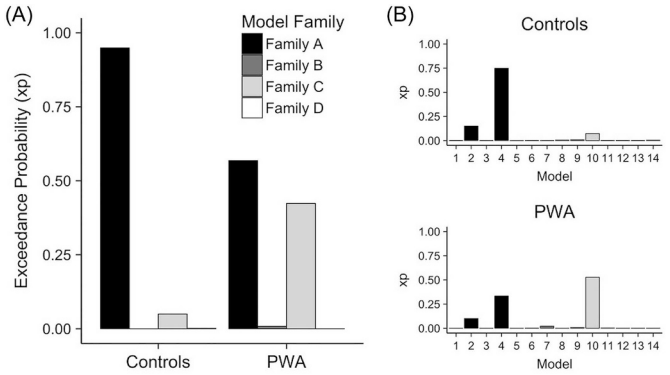

Fig. 6. Model fit. (A) Family-wise Bayesian Model Selection (BMS) in both participant groups and individual model results in (B) controls (top) and patients (bottom).

damage—primarily included positive loadings of white matter tracts (i.e., LIFOF, LUF, LCCallosum and LaCommissure) as well as STGpole. These five lesion components were used as independent variables in subsequent analyses reported below.

3.5.1. Relationship between effective connections and lesion variables

Separate backward stepwise regression models were run to determine if lesion variables (i.e., LC1: Dorsal damage, LC2: Ventral damage, LC3: Parietal damage, LC4: Superior frontal damage, LC5: WM damage and total lesion volume) predicted connectivity, as captured by the five DCM components (i.e., CC1: RH connectivity; CC2: Target bilateral frontal ROIs; CC3: IntraLH, target frontal; CC4: IntraLH, target LITG and CC5: Target bilateral posterior ROIs). The full results of final models are shown in Table 5. Significant independent lesion predictors of each DCM component are illustrated in Fig. 9.

The following significant relationships emerged. First, the overall model predicting CC1: RH connectivity was significant ($F(3,26) = 4.48$, $p = .012$) and explained approximately 34% of the variance in these connectivity parameters. With all other variables within this model held constant, higher CC1: RH connectivity was significantly predicted by greater damage to structures that loaded onto LC4: Superior frontal damage (i.e., LPreCG, LMFG and LCCallosum) ($\beta = 0.404$, $t = 2.535$, $p = .018$). A trending association between less damage to ROIs that loaded onto LC5: WM damage (most notably ventral association and commissural white matter tracts) and higher CC1: RH connectivity was also observed ($\beta = -0.315$, $t = -1.976$, $p = .059$) with LC3 and LC4 held constant.

When CC2: Target bilateral frontal ROIs was the dependent variable, backward stepwise regression yielded an intercept-only model, indicating that none of the lesion variables were related to the strength of these connections. By contrast, the final model predicting CC3: IntraLH, target frontal ROIs was significant ($F(3,26) = 3.15$, $p = .042$) and explained approximately 27% of the variance in these connectivity parameters. Within this model, greater CC3: IntraLH, target frontal ROI connectivity was associated with higher LC2: Ventral damage ($\beta = 0.529$, $t = 2.705$, $p = .012$) and lower total lesion volume ($\beta = -5.853^{-06}$, $t = -2.269$, $p = .032$) when other variables within the model were held constant.

Next, the final model for CC4: IntraLH, target LITG was also significant ($F(2,27) = 3.91$, $p = .032$) and explained approximately 23% of the variance in CC4. With LC1 scores held constant within the model, lesion volume was the only independent predictor ($\beta = 7.417^{-06}$, $t = 2.797$, $p = .009$), indicating that patients with greater overall left hemisphere damage demonstrated stronger connectivity of connections in which LITG was modulated by other left hemisphere ROIs. Last, the overall model for CC5: Target bilateral posterior ROIs was significant ($F(4,25) = 3.32$, $p = .026$), explaining around 35% of the variance in the data. When other variables within the model were held constant,

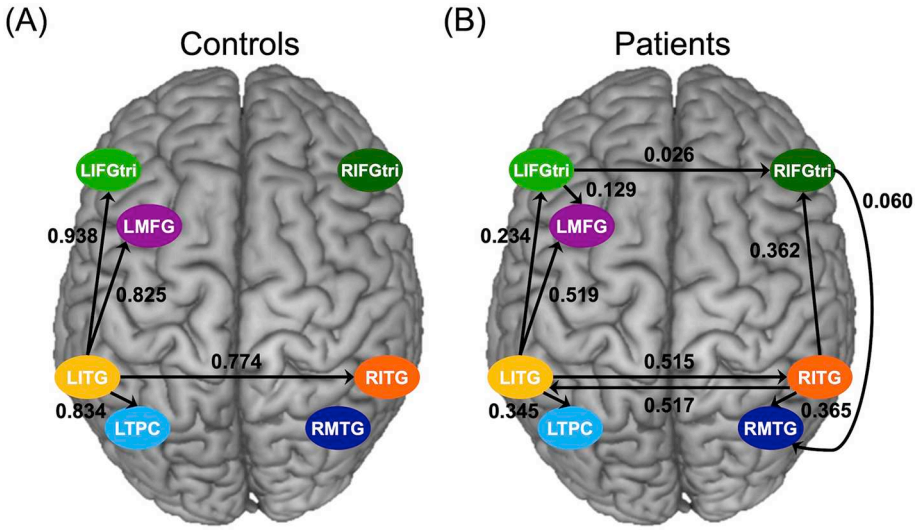

Fig. 7. Task-modulated connectivity. Significant connections in (A) controls and (B) patients where the arrowhead indicates the direction of the connection between regions and the parameter value is shown in Hertz.

Table 4
Summary of between-group comparisons in task-modulated DCM parameters.

	(df) F-stat	Parameter strength in Hz (mean ± SD)	Unadjusted p-values	BH-adjusted p-values
Left intrahemispheric	**(12,34) 3.518**	**–**	**0.002****	**0.006****
LIFGtri ➔ LITG	(1,45) 0.000	HC: 0.032 ± 0.248 PWA: 0.034 ± 0.209	0.978	0.978
LIFGtri ➔ LMFG	(1,45) 0.327	HC: 0.098 ± 0.226 PWA: 0.129 ± 0.351	0.570	0.760
LIFGtri ➔ LTPC	(1,45) 3.719	HC: 0.157 ± 0.458 PWA: -0.034 ± 0.075	0.060ˆ	0.120
LITG ➔ LIFGtri	(1,45) 18.826	HC: 0.938 ± 0.709 PWA: 0.234 ± 0.444	< 0.001***	0.001**
LITG ➔ LMFG	(1,45) 3.836	HC: 0.824 ± 0.465 PWA: 0.519 ± 0.504	0.056ˆ	0.120
LITG ➔ LTPC	(1,45) 9.393	HC: 0.834 ± 0.591 PWA: 0.345 ± 0.503	0.004**	0.022*
LMFG ➔ LIFGtri	(1,45) 1.147	HC: -0.040 ± 0.239 PWA: 0.048 ± 0.239	0.290	0.435
LMFG ➔ LITG	(1,45) 5.631	HC: -0.196 ± 0.471 PWA: 0.086 ± 0.240	0.022*	0.086
LMFG ➔ LTPC	(1,45) 5.120	HC: 0.108 ± 0.372 PWA: -0.033 ± 0.151	0.029*	0.086
LTPC ➔ LIFGtri	(1,45) 0.138	HC: -0.019 ± 0.201 PWA: 0.007 ± 0.135	0.712	0.776
LTPC ➔ LITG	(1,45) 2.744	HC: -0.260 ± 1.105 PWA: 0.096 ± 0.183	0.105	0.179
LTPC ➔ LMFG	(1,45) 0.198	HC: 0.037 ± 0.248 PWA: 0.037 ± 0.108	0.659	0.776
Right intrahemispheric	**(6,40) 0.771**	**–**	**0.597**	**0.597**
RIFGtri ➔ RITG	(1,45) 2.641	HC: -0.032 ± 0.098 PWA: 0.095 ± 0.272	0.111	0.383
RIFGtri ➔ RMTG	(1,45) 0.044	HC: 0.062 ± 0.180 PWA: 0.060 ± 0.131	0.835	0.835
RITG ➔ RIFGtri	(1,45) 1.038	HC: 0.209 ± 0.422 PWA: 0.362 ± 0.653	0.314	0.627
RITG ➔ RMTG	(1,45) 0.074	HC: 0.317 ± 0.596 PWA: 0.364 ± 0.460	0.787	0.835
RMTG ➔ RIFGtri	(1,45) 0.063	HC: 0.023 ± 0.178 PWA: 0.036 ± 0.188	0.803	0.835
RMTG ➔ RITG	(1,45) 2.408	HC: -0.041 ± 0.196 PWA: 0.063 ± 0.206	0.128	0.383
Inter-hemispheric	**(6,40) 2.337**	**–**	**0.050ˆ**	**0.075ˆ**
LIFGtri ➔ RIFGtri	(1,45) 6.647	HC: 0.163 ± 0.247 PWA: 0.026 ± 0.121	0.013*	0.080
LITG ➔ RITG	(1,45) 3.396	HC: 0.774 ± 0.671 PWA: 0.515 ± 0.515	0.072ˆ	0.216
LMFG ➔ RIFGtri	(1,45) 1.672	HC: 0.001 ± 0.004 PWA: -0.001 ± 0.004	0.203	0.314
RIFGtri ➔ LIFGtri	(1,45) 1.621	HC: -0.080 ± 0.223 PWA: 0.101 ± 0.332	0.210	0.314
RIFGtri ➔ LITG	(1,45) 0.310	HC: -0.001 ± 0.004 PWA: -0.001 ± 0.004	0.581	0.581
RIFGtri ➔ LMFG	(1,45) 0.378	HC: 0.498 ± 0.581 PWA: 0.517 ± 0.399	0.542	0.581

Notes: Statistics for overall multivariate models (i.e., left intrahemispheric, right intrahemispheric and interhemispheric connections) are shown in bold font followed by univariate effects for each connection within each model. FDR correction via Benjamini-Hochberg (BH) method for three models. Significance for p-values: ˆ 0.08 < > 0.05, * < 0.05, ** < 0.01, *** < 0.001. Hz = Hertz, SD = standard deviation, HC = healthy controls, PWA = persons with aphasia.

significant independent predictors included LC5: WM damage ($\beta = 0.594$, $t = 3.385$, $p = .002$) and total lesion volume ($\beta = -8.528^{-06}$, $t = -2.515$, $p = .019$) with a trending prediction by LC1: Dorsal damage ($\beta = 0.443$, $t = 1.951$, $p = .062$). In other words, stronger CC5: Target bilateral posterior ROI connectivity was associated with smaller overall lesion volume but greater damage to LILF, LIFOF, the left portions of commissural tracts and left dorsal structures when these variables were considered together.

Follow-up analyses were conducted to determine whether noisy VOIs influenced the relationships between DCM and lesion components. Of the seven regions included in the DCM analysis, a noisy signal was extracted for more than one patient from LMFG, LIFGtri, LTPC and RIFGtri. As shown in Supplementary Table S3, significant relationships were not found between most DCM components and binary noisy VOI variables. Exceptions included significant relationships between CC4: IntraLH, target LITG and noisy LMFG VOIs ($r = 0.455$, $p = .011$, uncorrected) as well as CC5: Target bilateral posterior ROIs and noisy LTPC VOIs ($r = -0.575$, $p < .001$, uncorrected). As shown in Supplementary Table S4, when the CC4: IntraLH, target LITG regression model was re-run controlling for noisy LMFG VOIs, the overall model remained significant ($F(3,26) = 3.26$, $p = .037$); consistent with the previous results, total lesion volume remained the only significant independent predictor ($\beta = 6.636^{-06}$, $t = 2.475$, $p = .020$) when other model variables were held constant. When the CC5: Target bilateral posterior ROIs regression model was re-run controlling for noisy LTPC VOIs, the multivariate model was signficant ($F(5,24) = 3.54$, $p = .015$), but none of the variables were significant independent predictors when included within the same model. Thus, it can be inferred that noisy LTPC VOIs (that were extracted due to highly damaged LTPC masks) and other previously-significant predictors in the model (i.e., lesion PC5

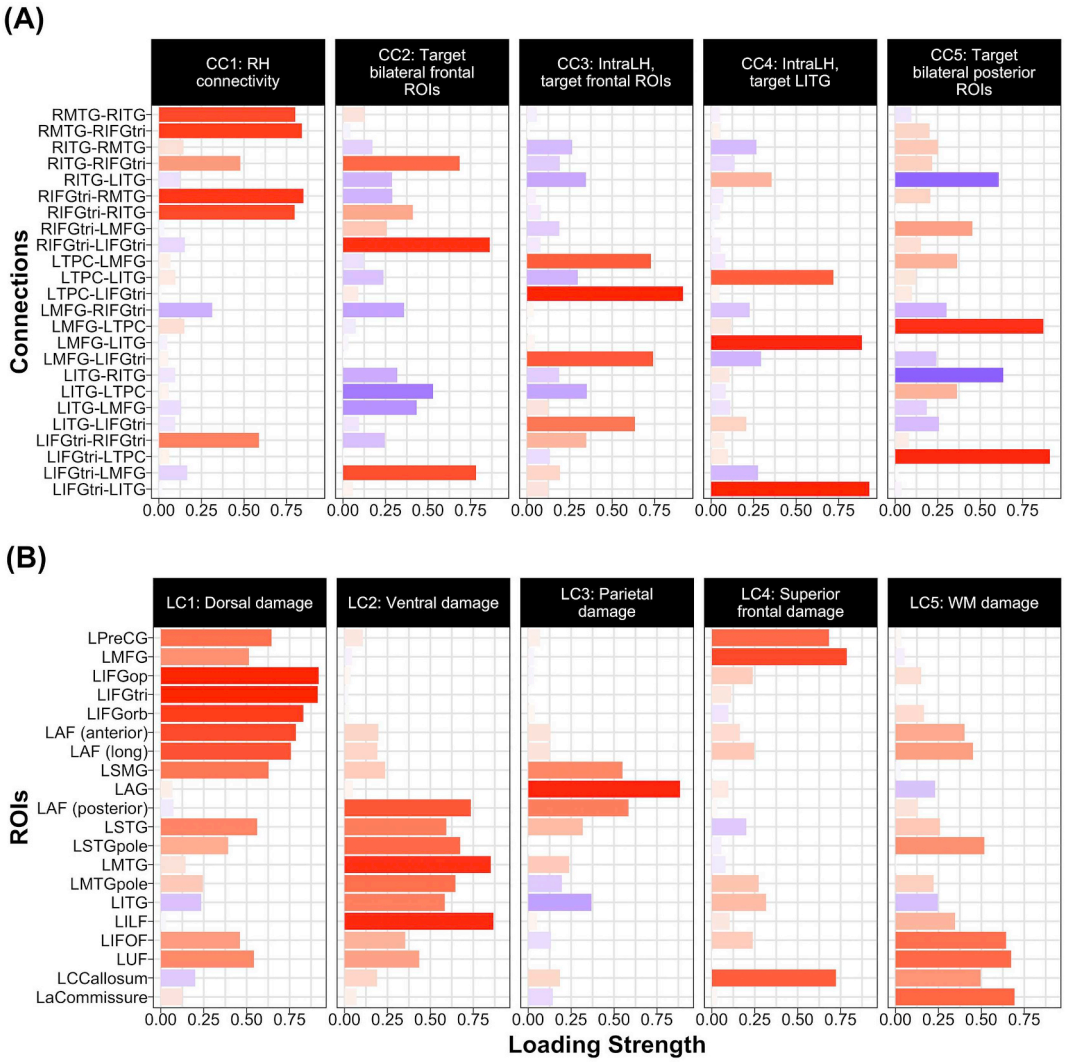

Fig. 8. Loadings onto PCA components for (A) DCM connection parameters and (B) regional percentage of damage. Positive and negative loadings are shaded in red and blue, respectively. CC = connectivity component, LC = lesion component, RH = Right hemisphere, ROIs = regions of interest, IntraLH = left intrahemispheric connections, WM = white matter.

Table 5
Summary of backward stepwise regressions predicting five DCM connection components from lesion variables.

	Overall model				
DCM Variable	(df) *F-stat*	*p-value*	R^2	Lesion Predictors	*p-value*
CC1: RH connectivity	(3,26) *4.48*	0.012*	0.341	LC3: $\beta = -0.280$, t = −1.759	0.090
				LC4: $\beta = 0.404$, t = 2.535	0.018*
				LC5: $\beta = -0.315$, t = −1.976	0.059ˆ
CC2: Target bilateral frontal ROIs	–	–	–	–	–
CC3: IntraLH, target frontal ROIs	(3,26) *3.15*	0.042*	0.266	LC2: $\beta = 0.529$, t = 2.705	0.012*
				LC3: $\beta = 0.311$, t = 1.738	0.094
				Vol.: $\beta = -5.853^{-06}$, t = −2.269	0.032*
CC4: IntraLH, target LITG	(2,27) *3.91*	0.032*	0.225	LC1: $\beta = -0.353$, t = −1.680	0.104
				Vol.: $\beta = 7.417^{-06}$, t = 2.797	0.009**
CC5: Target bilateral posterior ROIs	(4,25) *3.32*	0.026*	0.347	LC1: $\beta = 0.443$, t = 1.951	0.062ˆ
				LC4: $\beta = 0.360$, t = 1.751	0.092
				LC5: $\beta = 0.594$, t = 3.385	0.002**
				Vol.: $\beta = -8.528^{-06}$, t = −2.515	0.019*

Notes: Dashes indicate intercept-only model for DCM PC2 predicted by lesion variables. CC = connectivity component, LC = lesion component, RH = Right hemisphere, ROIs = regions of interest, IntraLH = left intrahemispheric connections, Vol. = total lesion volume. Variance inflation factors (VIFs) for all models were < 3.0. Significance for *p*-values: ˆ 0.08 < > 0.05, * < 0.05, ** < 0.01, *** < 0.001.

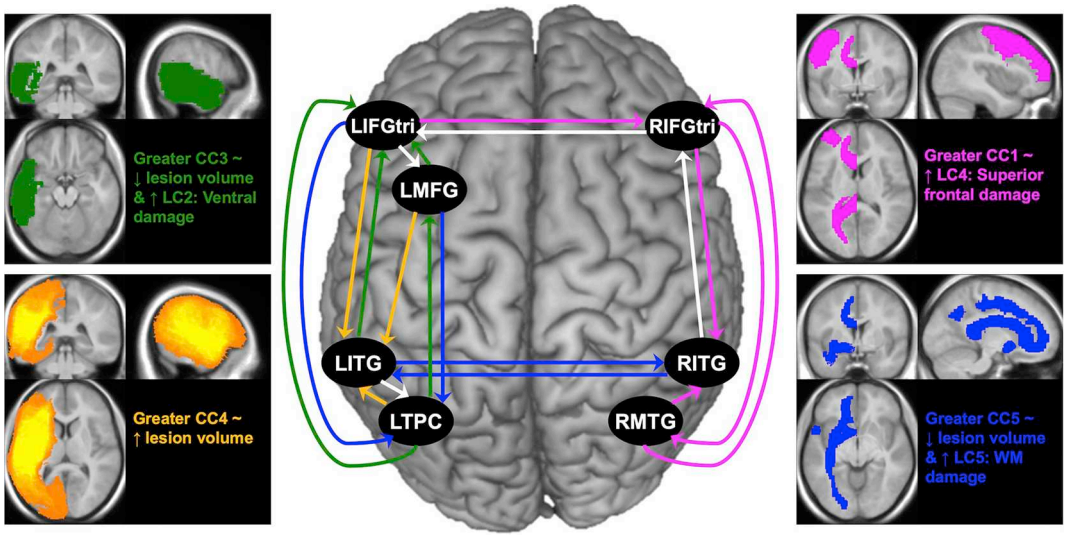

Fig. 9. Lesion predictors of DCM components. In the central image, colored arrows reflect connections that heavily loaded onto components (at $-0.50 \leq$ or ≥ 0.50), where pink = CC1: RH connectivity; white = CC2: Target bilateral frontal ROIs; green = CC3: IntraLH, target frontal ROIs; yellow = CC4: IntraLH, target LITG; and blue = CC5: Target bilateral posterior ROI connections. The images and colored text at the far left and right illustrate significant lesion predictors of each DCM connection component ($p < .05$) from regression models summarized in Table 5, where LC = lesion component, ~ = associated with, ↑ = higher, ↓ = lower.

Table 6
Summary of backward stepwise regressions predicting language abilities from DCM connection and lesion components.

	Overall model				
Variable	(df) *F-stat*	*p-value*	R^2	DCM & Lesion Predictors	*p-value*
fMRI task %acc	(4,25) *2.74*	0.051ˆ	0.305	CC2: $\beta = 0.041$, t = 1.504	0.145
				CC5: β = -0.038, t = −1.356	0.187
				LC1: $\beta = -0.055$, t = −2.068	0.049*
				LC2: $\beta = -0.057$, t = −1.992	0.057ˆ
fMRI task RT^{exp}	(4,25) *4.44*	0.008**	0.416	CC2: $\beta = 0.753$, t = 2.078	0.048*
				CC3: $\beta = 0.843$, t = 2.330	0.028*
				CC5: $\beta = -0.732$, t = −1.998	0.057ˆ
				LC3: $\beta = 0.506$, t = 1.335	0.194
WAB-R AQ	(4,25) *5.50*	0.003**	0.468	CC4: $\beta = -5.410$, t = −1.502	0.146
				LC1: $\beta = -10.801$, t = −3.122	0.005**
				LC2: $\beta = -8.004$, t = −2.245	0.034*
				LC5: $\beta = -5.057$, t = −1.446	0.161

Notes: %acc = percent accuracy on the fMRI task, RT^{exp} = fMRI task RT in milliseconds, exponentiated (exp) to improve distribution of the residuals. CC = connectivity component, LC = lesion component. Variance inflation factors (VIFs) for all models were < 3.0. Significance for p-values: ˆ 0.08 < > 0.05, * < 0.05, ** < 0.01, *** < 0.001.

and total lesion volume) captured the same variance in CC5 connectivity.

3.5.2. Effective connectivity and lesion predictors of language skills

The final backward stepwise regression models[4] predicting language abilities from DCM and lesion components are summarized in Table 6. The final model for fMRI task accuracy was nearly significant ($F(4,25) = 2.74$, $p = .051$) and explained approximately 31% of the variance in task accuracy. Of the four factors retained in the final model, LC1: Dorsal damage was a significant predictor ($\beta = -0.055$, $t = -2.068$, $p = .049$) and LC2: Ventral damage trended towards significance ($\beta = -0.057$, $t = -1.992$, $p = .057$) when other model variables were held constant.

The final model predicting RT^{exp} from DCM and lesion components was significant ($F(4,25) = 4.44$, $p = .008$) and included four predictors that explained approximately 42% of the variance in reaction time. Within this model, longer RTs were significantly related to greater connectivity of CC2: Target bilateral frontal ROIs ($\beta = 0.753$, $t = 2.078$, $p = .048$) (when CC3, CC5 and LC3 were held constant) and CC3: IntraLH, target frontal ROIs ($\beta = 0.843$, $t = 2.330$, $p = .028$) (when CC2, CC5 and LC3 were held constant). With the other component scores included in the model held constant, higher connectivity of CC5: Target bilateral posterior ROIs trended towards lower RT^{exp} ($\beta = -0.732$, $t = -1.998$, p = .057).

For WAB-R AQ, the final model was also significant ($F(4,25) = 5.50$, $p = .003$) and included one DCM and three lesion components that explained approximately 47% of the variance in aphasia severity. With the other lesion variables and CC4 held constant, significant independent predictors included LC1: Dorsal damage ($\beta = -10.801$, $t = -3.122$, $p = .005$) and LC2: Ventral damage ($\beta = -8.004$, $t = -2.245$, $p = .034$), indicating that greater damage to structures throughout the left hemisphere is related to more severe aphasia. The implications of specific findings regarding connectivity and lesion

[4] To supplement regression models, Supplementary Figure S5 shows the correlation matrix between each language variable, each DCM connection component, each lesion component and total lesion volume.

predictors of language skills are discussed in greater detail below.

4. Discussion

The overarching aims of this study were to determine differences in lexical-semantic task-based connectivity between patients with chronic aphasia and healthy controls and to investigate whether a lesion- and connectivity-based hierarchical model of language conforms to patterns of chronic aphasia recovery documented in the patient literature. At the level of network models, controls demonstrated the predicted preference for models in Family A: Left-lateralized connectivity (i.e., no/minimal damage) whereas patients demonstrated an unexpected split preference for Family A and Family C: Bilateral posterior-weighted connectivity (i.e., anterior damage models). At the level of network connections, only connections within the left hemisphere were significantly modulated by the semantic feature judgment task for controls while several connections within and between both hemispheres were modulated by the task in PWA. Direct comparison of connectivity parameters revealed that PWA had significantly weaker left intrahemispheric task-modulated connectivity for certain connections (i.e., LITG➔LIFGtri, LITG➔LTPC) than did controls. Within PWA, the proposed hierarchical lesion-connectivity model (Fig. 1) was partially validated.

4.1. Differences between PWA and controls in bilateral lexical-semantic network connectivity

In terms of model-level inferences, the results in the healthy control group align with our predictions. Specifically, models within Family A: Left-lateralized connectivity were specifically created to mimic likely lexical-semantic connectivity patterns in healthy individuals, and these models were an excellent fit for the control data. Furthermore, the individual best-fit model for controls was model #4, a model that not only included full bidirectional left intrahemispheric connections but also modeled interhemispheric connections between prefrontal and inferior temporal regions. Older healthy individuals may rely on bilateral involvement during lexical-semantic tasks due to normal aging, an interpretation which has been suggested previously in the healthy aging literature (Baciu et al., 2016; Davis et al., 2014; Hoffman and Morcom, 2018; Manenti et al., 2013; Meinzer et al., 2009; Obler et al., 2010).

In PWA, best-fit model families partially aligned with predictions per our proposed hierarchy (see Fig. 1). If network characteristics were indeed completely driven by lesion size and location, we expected model fit to be split between Family B: Bilateral anterior-weighted connectivity (i.e., posterior damage models), Family C: Bilateral posterior-weighted connectivity (i.e., anterior damage models) and Family D: Right-lateralized connectivity (i.e., extensive left hemisphere damage). However, the best-fit family for PWA was Family A, followed by Family C with very low probability values for either Family B or D. Indeed, the individual models that best explained the patient group data belonged to these families: model #10 (from Family C) was the best-fit individual model across the patient group, followed by models #4 and #2 (from Family A). Model #10 was created to model potential functional reorganization (including bidirectional connections between LMFG-LTPC, LMFG-LITG, LMFG-RIFGtri and RIFGtri-RITG) in the face of damage to and disconnect from LIFGtri. On the other hand, models #2 and #4 were created to reflect different patterns of "normal" left-lateralized connectivity of an intact lexical-semantic system. While some patients (e.g., P1, P12 and P31) who demonstrated a preference for models #2 or #4 had relatively little damage to left hemisphere structures, other individuals (e.g., P5, P6 and P7) exhibited a notable degree of damage to frontal, temporal, and/or parietal regions, indicating that task-based connectivity was not entirely dictated by structural damage in these patients. This is a point that we return to and explore in greater detail in section, *4.2.1. Lesion and connectivity relationships in PWA*.

The parameter-level results yielded some similarities but also striking differences between patients and controls. In line with our hypotheses, the lexical-semantic task significantly modulated several left intrahemispheric connections in both controls and PWA, including connections in which LITG exerted a modulatory effect on other network ROIs (i.e., LMFG, LIFGtri, LTPC and RITG). These results make sense given that exogenous task input was modeled to LITG in most network models. These results may also reflect the importance of temporal cortex in general and inferior temporal regions in particular in lexical-semantic processing in healthy individuals (Binder et al., 2009; Price, 2012; Vigneau et al., 2006) and in PWA (Cloutman et al., 2009; DeLeon et al., 2007; Griffis et al., 2017a; Schwartz et al., 2009; Sims et al., 2016).

Also consistent with our predictions, certain left intrahemispheric task-modulated connections (i.e., LITG➔LIFGtri, LITG➔LTPC) were significantly stronger in controls compared to PWA, which aligns with results from other connectivity studies comparing patients with chronic aphasia to healthy individuals (Geranmayeh et al., 2016; Meier et al., 2016a; Sharp et al., 2010). Contrary to our predictions, patients did not recruit all LMFG-driven, intrahemispheric connections to a greater extent than did controls. In fact, at uncorrected statistical threshold, the results indicate that patients exhibited stronger excitatory connectivity of LMFG➔LITG than controls, but controls exhibited stronger excitatory connectivity of LMFG➔LTPC than did patients. Stronger excitatory coupling of LMFG➔LTPC in controls may reflect normal top-down modulation of lexical-semantic representations seen in healthy individuals (Binder and Desai, 2011; Xu et al., 2017) that patients lack. On the other hand, heightened modulation of LMFG➔LITG in PWA could be a consequence of damage to other left hemisphere regions, a hypothesis that is supported by the relationship between total lesion volume and LITG-modulated connections within this sample (see *4.2.1. Lesion and connectivity relationships in PWA*). Noteably, LMFG-driven connections were not significantly recruited in either group, a finding that is in direct contrast to Meier et al. (2018) but could be attributed to a variety of methodological differences between studies (e.g., modeling of nuisance regressors within the GLM, selection and localization of VOIs, modeling of regions within the model space, patients included in the DCM analyses, etc.).

Although the between-group comparisons of other connections did not reach statistical significance (possibly due to lack of power), the one-sample *t*-tests revealed that PWA significantly recruited additional connections that controls did not. Specifically, in patients, the semantic feature task significantly modulated more interhemispheric interactions, including LIFGtri➔RIFGtri and RITG➔LITG (see Fig. 7B). A significant connection from LIFGtri to LMFG was also observed in patients but not in controls, which may reflect the importance of intrahemispheric connectivity of left frontal regions that we asserted in our previous work (see Meier et al., 2018 but note the difference in directionality of LIFGtri and LMFG connectivity in that study). Finally, significant coupling between several regions within the right hemisphere was observed in the patients, as per our hypotheses. It is possible that patients recruited a broader network of connections to compensate for reduced functional coherence within the network due to functional and/or structural disconnection, which is one potential mechanism of neural reorganization in aphasia proposed by Abel et al. (2015). While this assertion cannot be confirmed, it is clear that the topology of the lexical-semantic network differed between controls and PWA.

4.2. The hierarchical lesion- and connectivity-based chronic aphasia recovery model: Revisited

One of the central goals of this study was to explicitly test whether lesion, connectivity and language profiles in PWA adhere to a recovery hierarchy similar to Heiss and Thiel (2006). Specifically, we examined potential relationships between lesion (left column in Fig. 1), effective connectivity (middle column in Fig. 1) and language performance (right

column in Fig. 1).

4.2.1. Lesion and connectivity relationships in PWA

As shown in Fig. 1, we proposed that damage to left hemisphere tissue in chronic aphasia results in shifts from normal, left intrahemispheric-lateralized connectivity patterns to heightened interhemispheric and right intrahemispheric connectivity. Consistent with this proposal, we found that damage to specific left hemisphere structures—primarily LPreCG, LMFG and corpus callosum—was significantly related to higher right intrahemispheric connectivity. This result aligns with previous literature citing links between brain damage and heightened contralesional connectivity or activity in patients with chronic stroke (Griffis et al., 2017a, 2017b; Heiss et al., 1999; Sandberg, 2017; Sims et al., 2016; Skipper-Kallal et al., 2017b, 2017a; Warren et al., 2009). Damage to specific left hemisphere structures was also associated with heightened intrahemispheric connectivity within presumed spared left hemisphere tissue. Specifically, greater damage to ventral temporal regions (i.e., LC2: Ventral damage) was associated with higher connectivity of left intrahemispheric connections involving modulation of left prefrontal regions (i.e., LMFG and LIFGtri). While this pattern was not explicitly modeled within our hierarchical recovery model, it is consistent with previous work demonstrating that damage to portions of left perisylvian language areas results in recruitment of spared ipsilesional tissue (Sebastian and Kiran, 2011; Sims et al., 2016; Skipper-Kallal et al., 2017b, 2017a).

Left intrahemispheric connectivity patterns were also altered in the face of greater total extent of left hemisphere damage. As expected, larger lesion volumes were associated with weaker connectivity of left intrahemispheric connections involving modulation of frontal regions (CC3: IntraLH, target frontal ROIs). Less expected was the relationship between greater lesion volume and stronger connections with LITG modulation (CC4: IntraLH, target LITG). Normal semantic feature task-modulated connectivity (as indicated by the control group) was characterized by the recruitment of LITG-*driven* connections to other left hemisphere regions; a highly-damaged left hemisphere may render LITG a non-functional, sole driver of left ROIs, resulting in heightened LITG-*modulated* connectivity in the patients.

Finally, the relationships between lesion and the two DCM components onto which bilateral intrahemispheric and interhemispheric connections loaded do not neatly fit within the hierarchical recovery model. We ultimately found that greater left intrahemispheric and interhemispheric modulation of posterior regions (CC5: Target bilateral posterior ROIs) was collectively predicted by a combination of factors (i.e., LC: WM damage, lesion volume and noisy LTPC VOIs), none of which independently predicted CC5: Target bilateral posterior ROI connectivity. This result likely reflects common lesion and connectivity patterns in individuals with noisy LTPC VOIs. Specifically, patients with highly-damaged left temporoparietal cortex have higher lesion volumes (relative to individuals without noisy LTPC VOIs) but relatively spared deep WM pathways and exhibit lower left intrahemispheric modulation of LTPC (i.e., LIFGtri➔LTPC and LMFG➔LTPC, which positively loaded on CC5) and higher bidirectional interhemispheric connectivity between LITG and RITG (connections which negatively loaded onto CC5). On the other hand, no significant relationships between lesion factors—lesion components or overall lesion volume—and CC2: Target bilateral frontal ROIs were found. The connections that loaded most heavily onto this component (LIFGtri➔LMFG, RIFGtri➔LIFGtri, RITG➔RIFGtri and LITG➔LMTG) are spatially distant, which may be one reason this subnetwork was not linked to the integrity of specific left hemisphere structures. It may be that regardless of lesion location or size, a general consequence of stroke in aphasia is increased recruitment of certain connections within and between both hemispheres to support language processing (see Fig. 7B). This hypothesis is consistent with the phenomenon of chronic hyperconnectivity following stroke, where additional functional detour paths are maintained in an effort to compensate for the loss of connectivity of network hubs (see Hillary and Grafman, 2017 for review).

In all, the lesion and connectivity results indicate that the broader lexical-semantic task-modulated network seen in PWA compared to controls was related to—but not entirely dictated by—lesion nor by the inclusion of noisy VOIs. For example, no relationships were found between lesion variables and the strength of connections that heavily loaded onto CC2: Target bilateral frontal ROIs, of which three connections (RITG➔RIFGtri, LIFGtri➔LMFG and LITG➔LTPC) were significantly recruited within the patient sample. By contrast, greater damage to left superior frontal structures was related to higher CC1: RH connectivity while damage to left ventral regions resulted in heightened connectivity of left intrahemispheric frontal-modulated connections. Greater total lesion volume was related to reduced connectivity of CC3: IntraLH, target frontal ROIs and CC5: Target bilateral posterior ROIs, consistent with the notion that general overall damage results in functional disconnection. Surprisingly, greater total lesion volume was associated with higher CC4: IntraLH, target LITG connectivity, a finding which may reflect deviation from normal lexical-semantic connectivity patterns in the event of extensive left hemisphere damage. Similar to patterns outlined in Fig. 1, these results indicate that connectivity shifts both to left and right intrahemispheric connections when insufficient tissue within the left hemisphere language network remains. How these lesion and connectivity patterns were related to patients' language abilities is addressed in the following section.

4.2.2. Lesion and connectivity differentially predict language skills in PWA

With regards to the relation between neuroimaging metrics and language performance, our approach entailed determining connectivity parameters and lesion factors that predicted fMRI task performance (per accuracy and RT) and overall aphasia severity (per WAB-R AQ). First, we found that lesion metrics significantly predicted both fMRI task accuracy and WAB-R AQ. Specifically, less frontal dorsal damage (i.e., LC1) was related to better accuracy on the fMRI task, which is consistent with our prior work (Meier et al., 2018; Sims et al., 2016) and with studies indicating that lesions to inferior frontal cortex in particular result in deficits of semantic control (e.g., Krieger-Redwood et al., 2015; Noonan et al., 2013; Whitney et al., 2011; Whitney et al., 2012). We also found strong negative associations between aphasia severity (WAB-R AQ) and LC1: Dorsal damage and LC2: Ventral damage. The inclusion of both these component variables within this model likely reflects overall lesion volume. Consistent with our hypotheses and prior studies (e.g., Forkel et al., 2014; Ivanova et al., 2016; Kertesz et al., 1979; Lazar and Antoniello, 2008), extensive left hemisphere damage resulted in more severe aphasia within the patient sample. Taken together, it may be that the integrity of specific brain structures—rather than the gross integrity of an entire hemisphere—is critical for determining the degree of specific linguistic impairments (Bonilha et al., 2014; Skipper-Kallal et al., 2017b) while lesion volume alone can serve as a sufficient proxy for global deficits associated with aphasia.

By contrast, connectivity components were the best predictors of fMRI task reaction time, a proxy for processing speed for lexical-semantic decision-making. Specifically, stronger connectivity of left intrahemisperic frontal-modulated (CC3: IntraLH, target frontal ROIs) and bilateral frontal-modulated (CC2: Target bilateral frontal ROIs) connections—and trending weaker connectivity of bilateral posterior-modulated connections (CC5: Target bilateral posterior ROIs)—predicted shorter RTs within the patient group. While direct relationships between fMRI task accuracy and DCM components were not found, it should be noted that shorter RTs were associated with lower accuracy on the fMRI task for patients ($r = 0.468$, $p = .009$). Considered together, the RT results suggest that PWA who were slow to respond during the task (but with good accuracy) had strong excitatory connectivity of connections that primarily involved the modulation of frontal regions (i.e., LIFGtri➔LMFG, RIFGtri➔LIFGtri, and RITG➔RIFGtri from CC2 and LITG➔LIFGtri, LMFG➔LIFGtri,

LTPC➔LIFGtri, LTPC➔LMFG from CC3). Heightened modulation of LIFGtri particularly coheres with studies that have suggested LIFG activity and/or connectivity is critical for tasks requiring semantic access or control, both in healthy individuals (e.g., Badre and D'Esposito, 2007; Badre et al., 2005; Devlin et al., 2003; Gold and Buckner, 2002; Noonan et al., 2013; Poldrack et al., 1999; Thompson-Schill et al., 1997; Wagner et al., 2001) and PWA (e.g., Abel et al., 2014, 2015; Fridriksson et al., 2010; Kiran et al., 2015; Marcotte et al., 2012; Rochon et al., 2010; Rosen et al., 2000; Sims et al., 2016; van Hees et al., 2014a; van Oers et al., 2010). On the other hand, patients who responded quickly (but with poor accuracy) exhibited strong connectivity of connections that positively loaded onto CC5: Target bilateral posterior ROIs (i.e., LIFGtri➔LTPC and LMFG➔LTPC). This result is more challenging to reconcile with the existing literature, given that other studies (e.g., Bonilha et al., 2017; Cloutman et al., 2009; DeLeon et al., 2007; Geranmayeh et al., 2017; Griffis et al., 2017b; Pillay et al., 2017; Schwartz et al., 2009; Skipper-Kallal et al., 2015; Walker et al., 2011) have highlighted the preservation and/or activation of left temporoparietal cortex in conserving patients' lexical-semantic abilities. For example, Skipper-Kallal et al. (2015) found that LTPC lesions resulted in an impaired ability to make relatedness judgments for abstract (but not concrete) words. Griffis et al. (2017a) found that patients with more preserved LTPC cortical and underlying white matter tissue demonstrated greater levels of distributed semantic task activation and that these factors positively predicted patient's language skills inside and outside the scanner. Nonetheless, in Meier et al. (2018), we also found that greater local activity of LpMTG—a region that overlapped the LTPC mask—was related to poor lexical-semantic skills on an out-of-scanner task, a finding which is compatible with the present result.

Overall, performance on the fMRI task (per accuracy and RT) was generally related to less damage to and greater task-modulated connectivity of frontal areas whereas overall aphasia severity was predicted best by spared tissue within left hemisphere ventral and dorsal ROIs—a proxy for overall lesion volume. While the relationships between lesion components and language variables were in line with our hypotheses, the fact that the DCM connection components were poor predictors of language abilities was not. In Meier et al. (2018), we found that greater accuracy on the semantic judgment fMRI task was related to stronger connectivity of LpMTG➔LIFGtri. This discrepancy could be attributed to the vastly different model spaces employed in the two investigations or to other methodological differences between the studies (e.g., modeling within the GLM, VOI identification, non-overlapping participants, and/or use of DCM components). Alternatively, it may be that the connectivity patterns within the patient group reflect processes not directly related to—or captured by—fMRI task accuracy. For example, Geranmayeh et al. (2014a) suggested that heightened or altered functional brain responses could reflect increased cognitive effort during language tasks in PWA, a phenomenon which can occur independent of task accuracy. In particular, the right intrahemispheric frontotemporal connections significantly recruited in PWA may indicate the recruitment of additional goal-directed attentional resources or working memory rather than lexical-semantic processing in itself (Geranmayeh et al., 2014b; Skipper-Kallal et al., 2017b; van Oers et al., 2010). DCM connections may instead reflect characteristics inherent to the functional topology of these regions in these patients that are not than specific to cognitive processes. This hypothesis is similar to a conclusion drawn by Skipper-Kallal et al. (2017b), where the authors hypothesized that certain activation patterns—or in the present study, connectivity patterns—may reflect reorganization of language networks established in earlier phases of aphasia recovery.

4.3. Limitations and future directions

What do the present findings mean for predictive modeling of chronic aphasia recovery? In the present study, lesion variables were strong predictors of both task-based connectivity and language abilities within patients. While the damaged tissue components allowed for more nuanced interpretations regarding the effect of lesion than total lesion volume alone, the selected ROIs did not cover the entire brain. Thus, meaningful lesion information may have been excluded from these analyses. Challenges in defining and using lesion variables to predict individual aphasia recovery have been previously highlighted (Price et al., 2017), but the inclusion of functional metrics into recovery models may be frought with even more issues. Unlike lesion measures—which are static and unchanging—functional metrics are dynamic and can be easily influenced by factors unrelated to aphasia severity or general recovery. In the present study, for example, we used a semantic feature judgment task—which required participants to view pictures, read written features and make judgments regarding those features—as a proxy for the language network. It is possible that different results (e.g., less reliance on LITG connectivity) could have been attained had a different task been utilized.

Moreover, functional and effective connectivity results depend to some extent on methodology, and presently, there is no gold standard for how to perform connectivity modeling in chronic aphasia. For example, the use of the noisy VOI methodology in the present study meant that the relationships between lesion, language and connectivity were partially influenced by the presence of noisy signals, particularly for connections involving LTPC. However, the alternative would have been removing patients from the DCM analyses, an approach that has been utilized in previous DCM studies (Chu et al., 2018; Meier et al., 2016a), but results in the exclusion of patients representative of the larger aphasic population. Furthermore, connectivity methods like DCM are inherently ROI-based approaches and depend on the selection and modeling of regions. Therefore, the present results reflect the DCM model space used to test our specific hypotheses but do not necessarily reflect the “true” semantic network. Thus, to reach more definitive conclusions regarding lesion, connectivity and language ability patterns in PWA, replication of this study's primary aims with other types of language tasks, alternative connectivity methods, or even resting state fMRI—which shows particular promise in generating meaningful phenotypes of stroke deficit profiles (Carter et al., 2012; Hartwigsen and Saur, 2017; Klingbeil et al., 2017)—is warranted.

5. Conclusions

While the specific mechanisms of chronic aphasia recovery remain elusive, the findings of the present study indicate that neural recovery of language in chronic aphasia likely cannot be attributed entirely to one hemisphere of the brain versus the other. We found that a more nuanced hierarchical model that incorporates lesion, connectivity and specific linguistic measures may be useful in characterizing aphasia recovery. It appears that function—as measured by effective network methodologies—is not entirely driven by overt structural damage in patients. Multimodal imaging studies may best capture chronic aphasia recovery, yet much work is needed to determine optimal modeling of lesion, functional connectivity and language metrics.

Acknowledgments

We want to thank all individuals who participated in the present study, particularly the patients with aphasia for their time and effort in completing study procedures. We also extend our gratitude to past and present members of the Boston University Aphasia Research Laboratory and our collaborators who assisted with data collection and analysis, in particular Kushal Kapse, Yansong Geng, Jen Michaud, Kelly Martin, Natalie Gilmore, and Maria Dekhtyar.

Funding sources

This work was funded by the National Institutes of Health/National Institute on Deafness and Other Communication Disorders though

grants 1P50DC012283 and 1F31DC015940.

Declarations of interest

Dr. Kiran is a Scientific Consultant for The Learning Corporation, but there is no overlap between this role and the submitted investigation. The authors have no other declarations of interest.

Appendix A. Supplementary data

Supplementary data to this article can be found online at https://doi.org/10.1016/j.nicl.2019.101919.

References

Abel, S., Weiller, C., Huber, W., Willmes, K., 2014. Neural underpinnings for model-oriented therapy of aphasic word production. Neuropsychologia 57, 154–165. https://doi.org/10.1016/j.neuropsychologia.2014.03.010.

Abel, S., Weiller, C., Huber, W., Willmes, K., Specht, K., 2015. Therapy-induced brain reorganization patterns in aphasia. Brain 138 (4), 1097–1112. https://doi.org/10.1093/brain/awv022.

Abo, M., Senoo, A., Watanabe, S., Miyano, S., Doseki, K., Sasaki, N., Yonemoto, K., 2004. Language-related brain function during word repetition in post-stroke aphasics. Neuroreport 15 (12), 1891–1894.

Allendorfer, J.B., Kissela, B.M., Holland, S.K., Szaflarski, J.P., 2012. Different patterns of language activation in post-stroke aphasia are detected by overt and covert versions of the verb generation fMRI task. Med. Sci. Monitor 18 (3), CR135–137.

Ardila, A., Bernal, B., Rosselli, M., 2016. Connectivity of BA46 involvement in the executive control of language. Psicothema 28 (1), 26–31. https://doi.org/10.7334/psicothema2015.174.

Baciu, M., Boudiaf, N., Cousin, E., Perrone-Bertolotti, M., Pichat, C., Fournet, N., Krainik, A., 2016. Functional MRI evidence for the decline of word retrieval and generation during normal aging. AGE 38 (1). https://doi.org/10.1007/s11357-015-9857-y.

Badre, D., D'Esposito, M., 2007. Functional magnetic resonance imaging evidence for a hierarchical organization of the prefrontal cortex. J. Cogn. Neurosci. 19 (12), 2082–2099.

Badre, D., Poldrack, R.A., Paré-Blagoev, E.J., Insler, R.Z., Wagner, A.D., 2005. Dissociable controlled retrieval and generalized selection mechanisms in ventrolateral prefrontal cortex. Neuron 47 (6), 907–918. https://doi.org/10.1016/j.neuron.2005.07.023.

Barlow, T., 1877. On a case of double hemiplegia, with cerebral symmetrical lesions. Br. Med. J. 2 (865), 103–104.

Basso, A., Gardelli, M., Grassi, M.P., Mariotti, M., 1989. The role of the right hemisphere in recovery from aphasia: two case studies. Cortex 25 (4), 555–566. https://doi.org/10.1016/S0010-9452(89)80017-6.

Belin, P., Zilbovicius, M., Remy, P., Francois, C., Guillaume, S., Chain, F., Samson, Y., 1996. Recovery from nonfluent aphasia after melodic intonation therapy a PET study. Neurology 47 (6), 1504–1511.

Benjamini, Y., Hochberg, Y., 1995. Controlling the false discovery rate: a practical and powerful approach to multiple testing. 57 (1), 289–300.

Binder, J.R., Desai, R.H., 2011. The neurobiology of semantic memory. Trends Cogn. Sci. 15 (11), 527–536. https://doi.org/10.1016/j.tics.2011.10.001.

Binder, J.R., Desai, R.H., Graves, W.W., Conant, L.L., 2009. Where is the semantic system? A critical review and meta-analysis of 120 functional neuroimaging studies. Cereb. Cortex 19 (12), 2767–2796. https://doi.org/10.1093/cercor/bhp055.

Binney, R.J., Parker, G.J., Ralph, M.A.L., 2012. Convergent connectivity and graded specialization in the rostral human temporal lobe as revealed by diffusion-weighted imaging probabilistic tractography. J. Cogn. Neurosci. 24 (10), 1998–2014.

Blank, S.C., Bird, H., Turkheimer, F., Wise, R.J., 2003. Speech production after stroke: the role of the right pars opercularis. Ann. Neurol. 54 (3), 310–320.

Blasi, V., Young, A.C., Tansy, A.P., Petersen, S.E., Snyder, A.Z., Corbetta, M., 2002. Word retrieval learning modulates right frontal cortex in patients with left frontal damage. Neuron 36 (1), 159–170.

Bonilha, L., Rorden, C., Fridriksson, J., 2014. Assessing the clinical effect of residual cortical disconnection after ischemic strokes. Stroke 45 (4), 988–993. https://doi.org/10.1161/STROKEAHA.113.004137.

Bonilha, L., Hillis, A.E., Hickok, G., den Ouden, D.B., Rorden, C., Fridriksson, J., 2017. Temporal lobe networks supporting the comprehension of spoken words. Brain 140 (9), 2370–2380. https://doi.org/10.1093/brain/awx169.

Breier, J.I., Maher, L.M., Novak, B., Papanicolaou, A.C., 2006. Functional imaging before and after constraint-induced language therapy for aphasia using magnetoencephalography. Neurocase 12 (6), 322–331. https://doi.org/10.1080/13554790601126054.

Brett, M., Leff, A.P., Rorden, C., Ashburner, J., 2001. Spatial normalization of brain images with focal lesions using cost function masking. NeuroImage 14 (2), 486–500. https://doi.org/10.1006/nimg.2001.0845.

Brett, M., Anton, J., Valabregue, R., Poline, J.B., 2002. Region of interest analysis using the MarsBar toolbox for SPM 99 16 (2), S497.

Brownsett, S.L.E., Warren, J.E., Geranmayeh, F., Woodhead, Z., Leech, R., Wise, R.J.S., 2014. Cognitive control and its impact on recovery from aphasic stroke. Brain 137 (1), 242–254. https://doi.org/10.1093/brain/awt289.

Cabeza, R., 2002. Hemispheric asymmetry reduction in older adults: the HAROLD model. Psychol. Aging 17 (1), 85–100. https://doi.org/10.1037//0882-7974.17.1.85.

Cao, Y., Vikingstad, E.M., George, K.P., Johnson, A.F., Welch, K.M.A., 1999. Cortical language activation in stroke patients recovering from aphasia with functional MRI. Stroke 30 (11), 2331–2340.

Cappa, S.F., Vallar, G., 1992. The role of the left and right hemispheres in recovery from aphasia. Aphasiology 6 (4), 359–372. https://doi.org/10.1080/02687039208248607.

Carter, A.R., Shulman, G.L., Corbetta, M., 2012. Why use a connectivity-based approach to study stroke and recovery of function? NeuroImage 62 (4), 2271–2280. https://doi.org/10.1016/j.neuroimage.2012.02.070.

Catani, M., Mesulam, M., 2008. The arcuate fasciculus and the disconnection theme in language and aphasia: history and current state. Cortex 44 (8), 953–961. https://doi.org/10.1016/j.cortex.2008.04.002.

Catani, M., Thiebaut de Schotten, M., 2008. A diffusion tensor imaging tractography atlas for virtual in vivo dissections. Cortex 44 (8), 1105–1132. https://doi.org/10.1016/j.cortex.2008.05.004.

Catani, M., Howard, R.J., Pajevic, S., Jones, D.K., 2002. Virtual in vivo interactive dissection of white matter fasciculi in the human brain. NeuroImage 17 (1), 77–94. https://doi.org/10.1006/nimg.2002.1136.

Catani, M., Jones, D.K., ffytche, D.H., 2005. Perisylvian language networks of the human brain. Ann. Neurol. 57 (1), 8–16. https://doi.org/10.1002/ana.20319.

Cherney, L.R., Small, S.L., 2006. Task-dependent changes in brain activation following therapy for nonfluent aphasia: discussion of two individual cases. J. Int. Neuropsychol. Soc. 12 (6), 828–842.

Chu, R., Meltzer, J.A., Bitan, T., 2018. Interhemispheric interactions during sentence comprehension in patients with aphasia. Cortex 109, 74–91. https://doi.org/10.1016/j.cortex.2018.08.022.

Cloutman, L., Gottesman, R., Chaudhry, P., Davis, C., Kleinman, J.T., Pawlak, M., Hillis, A.E., 2009. Where (in the brain) do semantic errors come from? Cortex 45 (5), 641–649. https://doi.org/10.1016/j.cortex.2008.05.013.

Cloutman, L.L., Lambon Ralph, M.A., 2012. Connectivity-based structural and functional parcellation of the human cortex using diffusion imaging and tractography. Front. Neuroanat. 6. https://doi.org/10.3389/fnana.2012.00034.

Coltheart, M., 1981. The MRC psycholinguistic database. The Quarterly Journal of Experimental Psychology Section A 33 (4), 497–505. https://doi.org/10.1080/14640748108400805.

Davis, S.W., Zhuang, J., Wright, P., Tyler, L.K., 2014. Age-related sensitivity to task-related modulation of language-processing networks. Neuropsychologia 63, 107–115. https://doi.org/10.1016/j.neuropsychologia.2014.08.017.

DeLeon, J., Gottesman, R.F., Kleinman, J.T., Newhart, M., Davis, C., Heidler-Gary, J., Hillis, A.E., 2007. Neural regions essential for distinct cognitive processes underlying picture naming. Brain 130 (5), 1408–1422. https://doi.org/10.1093/brain/awm011.

Devlin, J.T., Matthews, P.M., Rushworth, M.F., 2003. Semantic processing in the left inferior prefrontal cortex: a combined functional magnetic resonance imaging and transcranial magnetic stimulation study. J. Cogn. Neurosci. 15 (1), 71–84.

Dinno, A., 2012. Paran: Horn's Test of Principal Components/Factors (Version R Package Version 1.5.1). Retrieved from. https://CRAN.R-project.org/package=paran.

Fedorenko, E., Behr, M.K., Kanwisher, N., 2011. Functional specificity for high-level linguistic processing in the human brain. Proc. Natl. Acad. Sci. 108 (39), 16428–16433. https://doi.org/10.1073/pnas.1112937108.

Fedorenko, E., Duncan, J., Kanwisher, N., 2012. Language-selective and domain-general regions lie side by side within Broca's area. Curr. Biol. 22 (21), 2059–2062. https://doi.org/10.1016/j.cub.2012.09.011.

Fedorenko, E., Duncan, J., Kanwisher, N., 2013. Broad domain generality in focal regions of frontal and parietal cortex. Proc. Natl. Acad. Sci. 110 (41), 16616–16621. https://doi.org/10.1073/pnas.1315235110.

Forkel, S.J., Thiebaut de Schotten, M., Dell'Acqua, F., Kalra, L., Murphy, D.G.M., Williams, S.C.R., Catani, M., 2014. Anatomical predictors of aphasia recovery: a tractography study of bilateral perisylvian language networks. Brain 137 (7), 2027–2039. https://doi.org/10.1093/brain/awu113.

Fox, J., Weisburg, S., 2011. *An {R} Companion to Applied Regression* (Second). Retrieved from. http://socserv.socsci.mcmaster.ca/jfox/Books/Companion.

Frey, S., Campbell, J.S.W., Pike, G.B., Petrides, M., 2008. Dissociating the human language pathways with high angular resolution diffusion fiber tractography. J. Neurosci. 28 (45), 11435–11444. https://doi.org/10.1523/JNEUROSCI.2388-08.2008.

Fridriksson, J., 2010. Preservation and modulation of specific left hemisphere regions is vital for treated recovery from anomia in stroke. J. Neurosci. 30 (35), 11558–11564. https://doi.org/10.1523/JNEUROSCI.2227-10.2010.

Fridriksson, J., Bonilha, L., Baker, J.M., Moser, D., Rorden, C., 2010. Activity in preserved left hemisphere regions predicts anomia severity in aphasia. Cereb. Cortex 20 (5), 1013–1019. https://doi.org/10.1093/cercor/bhp160.

Fridriksson, J., Richardson, J.D., Fillmore, P., Cai, B., 2012. Left hemisphere plasticity and aphasia recovery. NeuroImage 60 (2), 854–863. https://doi.org/10.1016/j.neuroimage.2011.12.057.

Friederici, A.D., Gierhan, S.M., 2013. The language network. Curr. Opin. Neurobiol. 23 (2), 250–254. https://doi.org/10.1016/j.conb.2012.10.002.

Friston, K.J., Harrison, L., Penny, W., 2003. Dynamic causal modelling. NeuroImage 19 (4), 1273–1302. https://doi.org/10.1016/S1053-8119(03)00202-7.

Gabrieli, J.D., Poldrack, R.A., Desmond, J.E., 1998. The role of left prefrontal cortex in language and memory. Proc. Natl. Acad. Sci. U. S. A. 95 (3), 906–913.

Geranmayeh, F., Brownsett, S.L.E., Wise, R.J.S., 2014a. Task-induced brain activity in aphasic stroke patients: what is driving recovery? Brain 137 (10), 2632–2648. https://doi.org/10.1093/brain/awu163.

Geranmayeh, F., Wise, R.J.S., Mehta, A., Leech, R., 2014b. Overlapping networks engaged during spoken language production and its cognitive control. J. Neurosci. 34 (26),

8728–8740. https://doi.org/10.1523/JNEUROSCI.0428-14.2014.
Geranmayeh, F., Leech, R., Wise, R.J., 2016. Network dysfunction predicts speech production after left hemisphere stroke. Neurology 86 (14), 1296–1305.
Geranmayeh, F., Chau, T.W., Wise, R.J.S., Leech, R., Hampshire, A., 2017. Domain-general subregions of the medial prefrontal cortex contribute to recovery of language after stroke. Brain 140 (7), 1947–1958. https://doi.org/10.1093/brain/awx134.
Glasser, M.F., Rilling, J.K., 2008. DTI tractography of the human brain's language pathways. Cereb. Cortex 18 (11), 2471–2482. https://doi.org/10.1093/cercor/bhn011.
Gold, B.T., Buckner, R.L., 2002. Common prefrontal regions coactivate with dissociable posterior regions during controlled semantic and phonological tasks. Neuron 35 (4), 803–812.
Griffis, J.C., Nenert, R., Allendorfer, J.B., Szaflarski, J.P., 2017a. Linking left hemispheric tissue preservation to fMRI language task activation in chronic stroke patients. Cortex 96, 1–18. https://doi.org/10.1016/j.cortex.2017.08.031.
Griffis, J.C., Nenert, R., Allendorfer, J.B., Vannest, J., Holland, S., Dietz, A., Szaflarski, J.P., 2017b. The canonical semantic network supports residual language function in chronic post-stroke aphasia. Hum. Brain Mapp. 38 (3), 1636–1658. https://doi.org/10.1002/hbm.23476.
Hartwigsen, G., Saur, D., 2017. Neuroimaging of stroke recovery from aphasia – insights into plasticity of the human language network. NeuroImage. https://doi.org/10.1016/j.neuroimage.2017.11.056.
van Hees, S., McMahon, K., Angwin, A., de Zubicaray, G., Copland, D.A., 2014a. Neural activity associated with semantic versus phonological anomia treatments in aphasia. Brain Lang. 129, 47–57. https://doi.org/10.1016/j.bandl.2013.12.004.
Heiss, W.-D., Thiel, A., 2006. A proposed regional hierarchy in recovery of post-stroke aphasia. Brain Lang. 98 (1), 118–123. https://doi.org/10.1016/j.bandl.2006.02.002.
Heiss, W.D., Kessler, J., Thiel, A., Ghaemi, M., Karbe, H., 1999. Differential capacity of left and right hemispheric areas for compensation of poststroke aphasia. Ann. Neurol. 45 (4), 430–438.
Hillary, F.G., Grafman, J.H., 2017. Injured brains and adaptive networks: the benefits and costs of Hyperconnectivity. Trends Cogn. Sci. 21 (5), 385–401. https://doi.org/10.1016/j.tics.2017.03.003.
Hoffman, P., Morcom, A.M., 2018. Age-related changes in the neural networks supporting semantic cognition: a meta-analysis of 47 functional neuroimaging studies. Neurosci. Biobehav. Rev. 84, 134–150. https://doi.org/10.1016/j.neubiorev.2017.11.010.
Hope, T.M.H., Seghier, M.L., Leff, A.P., Price, C.J., 2013. Predicting outcome and recovery after stroke with lesions extracted from MRI images. NeuroImage: Clinical 2, 424–433. https://doi.org/10.1016/j.nicl.2013.03.005.
Howard, D., Patterson, K.E., 1992. The Pyramids and Palm Trees Test: A Test of Semantic Access from Words and Pictures. Thames Valley Test Company.
Humphreys, G.F., Lambon Ralph, M.A., 2015. Fusion and fission of cognitive functions in the human parietal cortex. Cereb. Cortex 25 (10), 3547–3560. https://doi.org/10.1093/cercor/bhu198.
Indefrey, P., Levelt, W.J., 2000. The neural correlates of language production. In: The New Cognitive Neurosciences, 2nd. MIT Press, pp. 845–865.
Indefrey, P., Levelt, W.J.M., 2004. The spatial and temporal signatures of word production components. Cognition 92 (1–2), 101–144. https://doi.org/10.1016/j.cognition.2002.06.001.
Ivanova, M.V., Isaev, D.Y., Dragoy, O.V., Akinina, Y.S., Petrushevskiy, A.G., Fedina, O.N., Dronkers, N.F., 2016. Diffusion-tensor imaging of major white matter tracts and their role in language processing in aphasia. Cortex 85, 165–181. https://doi.org/10.1016/j.cortex.2016.04.019.
Kahan, J., Foltynie, T., 2013. Understanding DCM: ten simple rules for the clinician. NeuroImage 83, 542–549. https://doi.org/10.1016/j.neuroimage.2013.07.008.
Kaiser, H.F., 1960. The Application of Electronic Computers to Factor Analysis. 20. pp. 141–151.
Kaiser, H.F., Caffrey, J., 1965. Alpha factor analysis. Psychometrika 30 (1), 1–14. https://doi.org/10.1007/BF02289743.
Kaplan, E., Goodglass, H., Weintraub, S., Segal, O., & van Loon-Vervoorn, A. (2001). Boston Naming Test. (Pro-ed).
Kay, J., Coltheart, M., Lesser, R., 1992. Psycholinguistic Assessments of Language Processing in Aphasia, (PALPA): Auditory Processing. Lawrence Erlbaum Associates.
Kertesz, A., 2006. Western Aphasia Battery (Revised) PsychCorp. San Antonio, Tx. (Journal Article).
Kertesz, A., Harlock, W., Coates, R., 1979. Computer tomographic localization, lesion size, and prognosis in aphasia and nonverbal impairment. Brain Lang. 8 (1), 34–50.
Kiran, S., Meier, E.L., Kapse, K.J., Glynn, P.A., 2015. Changes in task-based effective connectivity in language networks following rehabilitation in post-stroke patients with aphasia. Front. Hum. Neurosci. 9. https://doi.org/10.3389/fnhum.2015.00316.
Klingbeil, J., Wawrzyniak, M., Stockert, A., Saur, D., 2017. Resting-state functional connectivity: an emerging method for the study of language networks in post-stroke aphasia. Brain Cogn. https://doi.org/10.1016/j.bandc.2017.08.005.
Krieger-Redwood, K., Teige, C., Davey, J., Hymers, M., Jefferies, E., 2015. Conceptual control across modalities: graded specialisation for pictures and words in inferior frontal and posterior temporal cortex. Neuropsychologia 76, 92–107. https://doi.org/10.1016/j.neuropsychologia.2015.02.030.
Lazar, R.M., Antoniello, D., 2008. Variability in recovery from aphasia. Current Neurology and Neuroscience Reports 8 (6), 497–502.
Lazar, R.M., Speizer, A.E., Festa, J.R., Krakauer, J.W., Marshall, R.S., 2008. Variability in language recovery after first-time stroke. J. Neurol. Neurosurg. Psychiatry 79 (5), 530–534. https://doi.org/10.1136/jnnp.2007.122457.
Léger, A., Démonet, J.-F., Ruff, S., Aithamon, B., Touyeras, B., Puel, M., Cardebat, D., 2002. Neural substrates of spoken language rehabilitation in an aphasic patient: an fMRI study. NeuroImage 17 (1), 174–183. https://doi.org/10.1006/nimg.2002.1238.
Levine, D.N., Mohr, J.P., 1979. Language after bilateral cerebral infarctions: role of the minor hemisphere in speech. Neurology 29 (7), 927–938.
Manenti, R., Brambilla, M., Petesi, M., Miniussi, C., Cotelli, M., 2013. Compensatory networks to counteract the effects of ageing on language. Behav. Brain Res. 249, 22–27. https://doi.org/10.1016/j.bbr.2013.04.011.
Marcotte, K., Ansaldo, A., 2010. The neural correlates of semantic feature analysis in chronic aphasia: discordant patterns according to the etiology. Semin. Speech Lang. 31 (1), 052–063. https://doi.org/10.1055/s-0029-1244953.
Marcotte, K., Adrover-Roig, D., Damien, B., de Préaumont, M., Généreux, S., Hubert, M., Ansaldo, A.I., 2012. Therapy-induced neuroplasticity in chronic aphasia. Neuropsychologia 50 (8), 1776–1786. https://doi.org/10.1016/j.neuropsychologia.2012.04.001.
Marreiros, A.C., Kiebel, S.J., Friston, K.J., 2008. Dynamic causal modelling for fMRI: a two-state model. NeuroImage 39 (1), 269–278. https://doi.org/10.1016/j.neuroimage.2007.08.019.
Mattioli, F., Ambrosi, C., Mascaro, L., Scarpazza, C., Pasquali, P., Frugoni, M., Gasparotti, R., 2014. Early aphasia rehabilitation is associated with functional reactivation of the left inferior frontal gyrus. Stroke 45 (2), 545–552.
Meier, E.L., Kapse, K.J., Kiran, S., 2016a. The relationship between frontotemporal effective connectivity during picture naming, behavior, and preserved cortical tissue in chronic aphasia. Front. Hum. Neurosci. 10. https://doi.org/10.3389/fnhum.2016.00109.
Meier, E.L., Lo, M., Kiran, S., 2016b. Understanding semantic and phonological processing deficits in adults with aphasia: effects of category and typicality. Aphasiology 30 (6), 719–749. https://doi.org/10.1080/02687038.2015.1081137.
Meier, E.L., Johnson, J.P., Kiran, S., 2018. Left frontotemporal effective connectivity during semantic feature judgments in patients with chronic aphasia and age-matched healthy controls. Cortex. https://doi.org/10.1016/j.cortex.2018.08.006.
Meinzer, M., Flaisch, T., Breitenstein, C., Wienbruch, C., Elbert, T., Rockstroh, B., 2008. Functional re-recruitment of dysfunctional brain areas predicts language recovery in chronic aphasia. NeuroImage 39 (4), 2038–2046. https://doi.org/10.1016/j.neuroimage.2007.10.008.
Meinzer, M., Flaisch, T., Wilser, L., Eulitz, C., Rockstroh, B., Conway, T., Crosson, B., 2009. Neural signatures of semantic and phonemic fluency in young and old adults. J. Cogn. Neurosci. 21 (10), 2007–2018. https://doi.org/10.1162/jocn.2009.21219.
Meinzer, M., Beeson, P.M., Cappa, S., Crinion, J., Kiran, S., Saur, D., Thompson, C.K., 2013. Neuroimaging in aphasia treatment research: consensus and practical guidelines for data analysis. NeuroImage 73, 215–224. https://doi.org/10.1016/j.neuroimage.2012.02.058.
Menke, R., Meinzer, M., Kugel, H., Deppe, M., Baumgärtner, A., Schiffbauer, H., Breitenstein, C., 2009. Imaging short- and long-term training success in chronic aphasia. BMC Neurosci. 10 (1), 118. https://doi.org/10.1186/1471-2202-10-118.
Mohr, B., Difrancesco, S., Harrington, K., Evans, S., Pulvermüller, F., 2014. Changes of right-hemispheric activation after constraint-induced, intensive language action therapy in chronic aphasia: fMRI evidence from auditory semantic processing1. Front. Hum. Neurosci. 8. https://doi.org/10.3389/fnhum.2014.00919.
Musso, M., Weiller, C., Kiebel, S., Müller, S.P., Bülau, P., Rijntjes, M., 1999. Training-induced brain plasticity in aphasia. Brain J. Neurol. 122, 1781–1790 Pt 9.
Naeser, M.A., Martin, P.I., Baker, E.H., Hodge, S.M., Sczerzenie, S.E., Nicholas, M., Yurgelun-Todd, D., 2004. Overt propositional speech in chronic nonfluent aphasia studied with the dynamic susceptibility contrast fMRI method. NeuroImage 22 (1), 29–41. https://doi.org/10.1016/j.neuroimage.2003.11.016.
Noonan, K.A., Jefferies, E., Visser, M., Lambon Ralph, M.A., 2013. Going beyond inferior prefrontal involvement in semantic control: evidence for the additional contribution of dorsal angular gyrus and posterior middle temporal cortex. J. Cogn. Neurosci. 25 (11), 1824–1850. https://doi.org/10.1162/jocn_a_00442.
Obler, L.K., Rykhlevskaia, E., Schnyer, D., Clark-Cotton, M.R., Spiro III, A., Hyun, J., Albert, M.L., 2010. Bilateral brain regions associated with naming in older adults. Brain Lang. 113 (3), 113–123. https://doi.org/10.1016/j.bandl.2010.03.001.
van Oers, C.A.M.M., Vink, M., van Zandvoort, M.J.E., van der Worp, H.B., de Haan, E.H.F., Kappelle, L.J., Dijkhuizen, R.M., 2010. Contribution of the left and right inferior frontal gyrus in recovery from aphasia. A functional MRI study in stroke patients with preserved hemodynamic responsiveness. NeuroImage 49 (1), 885–893. https://doi.org/10.1016/j.neuroimage.2009.08.057.
Parker, G.J.M., Luzzi, S., Alexander, D.C., Wheeler-Kingshott, C.A.M., Ciccarelli, O., Lambon Ralph, M.A., 2005. Lateralization of ventral and dorsal auditory-language pathways in the human brain. NeuroImage 24 (3), 656–666. https://doi.org/10.1016/j.neuroimage.2004.08.047.
Pena, E.A., Slate, E.H., 2014. Gvlma: Global Validation of Linear Models Assumptions (Version R Package Version 1.0.0.2). Retrieved from. https://CRAN.R-project.org/package=gvlma.
Penny, W.D., Stephan, K.E., Mechelli, A., Friston, K.J., 2004. Comparing dynamic causal models. NeuroImage 22 (3), 1157–1172. https://doi.org/10.1016/j.neuroimage.2004.03.026.
Penny, W.D., Stephan, K.E., Daunizeau, J., Rosa, M.J., Friston, K.J., Schofield, T.M., Leff, A.P., 2010. Comparing families of dynamic causal models. PLoS Comput. Biol. 6 (3), e1000709. https://doi.org/10.1371/journal.pcbi.1000709.
Pillay, S.B., Binder, J.R., Humphries, C., Gross, W.L., Book, D.S., 2017. Lesion localization of speech comprehension deficits in chronic aphasia. Neurology 88 (10), 970–975. https://doi.org/10.1212/WNL.0000000000003683.
Poldrack, R.A., Wagner, A.D., Prull, M.W., Desmond, J.E., Glover, G.H., Gabrieli, J.D., 1999. Functional specialization for semantic and phonological processing in the left inferior prefrontal cortex. NeuroImage 10 (1), 15–35. https://doi.org/10.1006/nimg.1999.0441.
Postman-Caucheteux, W.A., Birn, R.M., Pursley, R.H., Butman, J.A., Solomon, J.M., Picchioni, D., Braun, A.R., 2010. Single-trial fMRI shows contralesional activity linked to overt naming errors in chronic aphasic patients. J. Cogn. Neurosci. 22 (6), 1299–1318. https://doi.org/10.1162/jocn.2009.21261.

Price, C.J., 2010. The anatomy of language: a review of 100 fMRI studies published in 2009. Ann. N. Y. Acad. Sci. 1191 (1), 62–88. https://doi.org/10.1111/j.1749-6632.2010.05444.x.
Price, C.J., 2012. A review and synthesis of the first 20years of PET and fMRI studies of heard speech, spoken language and reading. NeuroImage 62 (2), 816–847. https://doi.org/10.1016/j.neuroimage.2012.04.062.
Price, C.J., Crinion, J., 2005. The latest on functional imaging studies of aphasic stroke. Curr. Opin. Neurol. 18 (4), 429–434.
Price, C.J., Devlin, J.T., Moore, C.J., Morton, C., Laird, A.R., 2005. Meta-analyses of object naming: effect of baseline. Hum. Brain Mapp. 25 (1), 70–82. https://doi.org/10.1002/hbm.20132.
Price, C.J., Hope, T.M., Seghier, M.L., 2017. Ten problems and solutions when predicting individual outcome from lesion site after stroke. NeuroImage 145, 200–208. https://doi.org/10.1016/j.neuroimage.2016.08.006.
Raboyeau, G., De Boissezon, X., Marie, N., Balduyck, S., Puel, M., Bezy, C., Cardebat, D., 2008. Right hemisphere activation in recovery from aphasia lesion effect or function recruitment? Neurology 70 (4), 290–298.
Richter, M., Miltner, W.H.R., Straube, T., 2008. Association between therapy outcome and right-hemispheric activation in chronic aphasia. Brain 131 (5), 1391–1401. https://doi.org/10.1093/brain/awn043.
Rochon, E., Leonard, C., Burianova, H., Laird, L., Soros, P., Graham, S., Grady, C., 2010. Neural changes after phonological treatment for anomia: an fMRI study. Brain Lang. 114 (3), 164–179. https://doi.org/10.1016/j.bandl.2010.05.005.
Rosen, H.J., Petersen, S.E., Linenweber, M.R., Snyder, A.Z., White, D.A., Chapman, L., Corbetta, M., 2000. Neural correlates of recovery from aphasia after damage to left inferior frontal cortex. Neurology 55 (12), 1883–1894.
Sandberg, C.W., 2017. Hypoconnectivity of resting-state networks in persons with aphasia compared with healthy age-matched adults. Front. Hum. Neurosci. 11. https://doi.org/10.3389/fnhum.2017.00091.
Sandberg, C.W., Bohland, J.W., Kiran, S., 2015. Changes in functional connectivity related to direct training and generalization effects of a word finding treatment in chronic aphasia. Brain Lang. 150, 103–116. https://doi.org/10.1016/j.bandl.2015.09.002.
Sarubbo, S., De Benedictis, A., Maldonado, I.L., Basso, G., Duffau, H., 2013. Frontal terminations for the inferior fronto-occipital fascicle: anatomical dissection, DTI study and functional considerations on a multi-component bundle. Brain Struct. Funct. 218 (1), 21–37. https://doi.org/10.1007/s00429-011-0372-3.
Saur, D., Lange, R., Baumgaertner, A., Schraknepper, V., Willmes, K., Rijntjes, M., Weiller, C., 2006. Dynamics of language reorganization after stroke. Brain 129 (6), 1371–1384. https://doi.org/10.1093/brain/awl090.
Saur, D., Kreher, B.W., Schnell, S., Kümmerer, D., Kellmeyer, P., Vry, M.-S., et al., 2008. Ventral and dorsal pathways for language. Proc. Natl. Acad. Sci. 105 (46), 18035–18040.
Schwartz, M.F., Kimberg, D.Y., Walker, G.M., Faseyitan, O., Brecher, A., Dell, G.S., Coslett, H.B., 2009. Anterior temporal involvement in semantic word retrieval: voxel-based lesion-symptom mapping evidence from aphasia. Brain 132 (12), 3411–3427. https://doi.org/10.1093/brain/awp284.
Sebastian, R., Kiran, S., 2011. Task-modulated neural activation patterns in chronic stroke patients with aphasia. Aphasiology 25 (8), 927–951. https://doi.org/10.1080/02687038.2011.557436.
Seghier, M.L., Zeidman, P., Neufeld, N.H., Leff, A.P., Price, C.J., 2010. Identifying abnormal connectivity in patients using dynamic causal modeling of FMRI responses. Front. Syst. Neurosci. 4. https://doi.org/10.3389/fnsys.2010.00142.
Seghier, M.L., Neufeld, N.H., Zeidman, P., Leff, A.P., Mechelli, A., Nagendran, A., Price, C.J., 2012. Reading without the left ventral occipito-temporal cortex. Neuropsychologia 50 (14), 3621–3635. https://doi.org/10.1016/j.neuropsychologia.2012.09.030.
Seghier, M.L., Bagdasaryan, J., Jung, D.E., Price, C.J., 2014. The importance of premotor cortex for supporting speech production after left capsular-putaminal damage. J. Neurosci. 34 (43), 14338–14348. https://doi.org/10.1523/JNEUROSCI.1954-14.2014.
Sharp, D.J., Turkheimer, F.E., Bose, S.K., Scott, S.K., Wise, R.J., 2010. Increased fronto-parietal integration after stroke and cognitive recovery. Ann. Neurol. 68 (5), 753–756.
Sims, J.A., Kapse, K., Glynn, P., Sandberg, C., Tripodis, Y., Kiran, S., 2016. The relationships between the amount of spared tissue, percent signal change, and accuracy in semantic processing in aphasia. Neuropsychologia 84, 113–126. https://doi.org/10.1016/j.neuropsychologia.2015.10.019.
Skipper-Kallal, L.M., Mirman, D., Olson, I.R., 2015. Converging evidence from fMRI and aphasia that the left temporoparietal cortex has an essential role in representing abstract semantic knowledge. Cortex 69, 104–120. https://doi.org/10.1016/j.cortex.2015.04.021.
Skipper-Kallal, L.M., Lacey, E.H., Xing, S., Turkeltaub, P.E., 2017a. Functional activation independently contributes to naming ability and relates to lesion site in post-stroke aphasia. Hum. Brain Mapp. 38 (4), 2051–2066. https://doi.org/10.1002/hbm.23504.
Skipper-Kallal, L.M., Lacey, E.H., Xing, S., Turkeltaub, P.E., 2017b. Right hemisphere remapping of naming functions depends on lesion size and location in poststroke aphasia. Neural Plasticity 2017, 1–17. https://doi.org/10.1155/2017/8740353.
Stephan, K.E., Penny, W.D., Moran, R.J., den Ouden, H.E.M., Daunizeau, J., Friston, K.J., 2010. Ten simple rules for dynamic causal modeling. NeuroImage 49 (4), 3099–3109. https://doi.org/10.1016/j.neuroimage.2009.11.015.
Stephan, K.E., Schlagenhauf, F., Huys, Q.J.M., Raman, S., Aponte, E.A., Brodersen, K.H., Heinz, A., 2017. Computational neuroimaging strategies for single patient predictions. NeuroImage 145, 180–199. https://doi.org/10.1016/j.neuroimage.2016.06.038.
Szaflarski, J.P., Eaton, K., Ball, A.L., Banks, C., Vannest, J., Allendorfer, J.B., Holland, S.K., 2011. Poststroke aphasia recovery assessed with functional magnetic resonance imaging and a picture identification task. J. Stroke Cerebrovasc. Dis. 20 (4), 336–345. https://doi.org/10.1016/j.jstrokecerebrovasdis.2010.02.003.
Szaflarski, J.P., Allendorfer, J.B., Banks, C., Vannest, J., Holland, S.K., 2013. Recovered vs. not-recovered from post-stroke aphasia: the contributions from the dominant and non-dominant hemispheres. Restor. Neurol. Neurosci. 31 (4), 347–360.
Thompson-Schill, S.L., D'Esposito, M., Aguirre, G.K., Farah, M.J., 1997. Role of left inferior prefrontal cortex in retrieval of semantic knowledge: a reevaluation. Proc. Natl. Acad. Sci. 94 (26), 14792–14797.
Turkeltaub, P.E., Messing, S., Norise, C., Hamilton, R.H., 2011. Are networks for residual language function and recovery consistent across aphasic patients? Neurology 76 (20), 1726–1734.
Turkeltaub, P.E., Coslett, H.B., Thomas, A.L., Faseyitan, O., Benson, J., Norise, C., Hamilton, R.H., 2012. The right hemisphere is not unitary in its role in aphasia recovery. Cortex 48 (9), 1179–1186. https://doi.org/10.1016/j.cortex.2011.06.010.
Turken, A.U., Dronkers, N.F., 2011. The neural architecture of the language comprehension network: converging evidence from lesion and connectivity analyses. Frontiers in System Neuroscience 5. https://doi.org/10.3389/fnsys.2011.00001.
Tzourio-Mazoyer, N., Landeau, B., Papathanassiou, D., Crivello, F., Etard, O., Delcroix, N., Joliot, M., 2002. Automated anatomical labeling of activations in SPM using a macroscopic anatomical parcellation of the MNI MRI single-subject brain. NeuroImage 15 (1), 273–289. https://doi.org/10.1006/nimg.2001.0978.
Van der Wouden, T., 1990. Celex: building a multifunctional polytheoretical lexical data base. Proceedings of BudaLex 88, 363–373.
Venables, W.N., Ripley, B.D., 2002. *Modern Applied Statistics with S* (Fourth). Retrieved from. http://www.stats.ox.ac.uk/pub/MASS4.
Vigneau, M., Beaucousin, V., Hervé, P.Y., Duffau, H., Crivello, F., Houdé, O., Tzourio-Mazoyer, N., 2006. Meta-analyzing left hemisphere language areas: phonology, semantics, and sentence processing. NeuroImage 30 (4), 1414–1432. https://doi.org/10.1016/j.neuroimage.2005.11.002.
Vigneau, M., Beaucousin, V., Hervé, P.-Y., Jobard, G., Petit, L., Crivello, F., Tzourio-Mazoyer, N., 2011. What is right-hemisphere contribution to phonological, lexico-semantic, and sentence processing? NeuroImage 54 (1), 577–593. https://doi.org/10.1016/j.neuroimage.2010.07.036.
Vitali, P., Abutalebi, J., Tettamanti, M., Danna, M., Ansaldo, A.-I., Perani, D., Cappa, S.F., 2007. Training-induced brain remapping in chronic aphasia: a pilot study. Neurorehabil. Neural Repair 21 (2), 152–160. https://doi.org/10.1177/1545968306294735.
Vitali, P., Tettamanti, M., Abutalebi, J., Ansaldo, A.-I., Perani, D., Cappa, S.F., Joanette, Y., 2010. Generalization of the effects of phonological training for anomia using structural equation modelling: a multiple single-case study. Neurocase 16 (2), 93–105. https://doi.org/10.1080/13554790903329117.
Wagner, A.D., Paré-Blagoev, E.J., Clark, J., Poldrack, R.A., 2001. Recovering meaning: left prefrontal cortex guides controlled semantic retrieval. Neuron 31 (2), 329–338.
Walker, G.M., Schwartz, M.F., Kimberg, D.Y., Faseyitan, O., Brecher, A., Dell, G.S., Coslett, H.B., 2011. Support for anterior temporal involvement in semantic error production in aphasia: new evidence from VLSM. Brain Lang. 117 (3), 110–122. https://doi.org/10.1016/j.bandl.2010.09.008.
Warburton, E., Price, C.J., Swinburn, K., Wise, R.J., 1999. Mechanisms of recovery from aphasia: evidence from positron emission tomography studies. J. Neurol. Neurosurg. Psychiatry 66 (2), 155–161.
Warren, J.E., Crinion, J.T., Lambon Ralph, M.A., Wise, R.J.S., 2009. Anterior temporal lobe connectivity correlates with functional outcome after aphasic stroke. Brain 132 (12), 3428–3442. https://doi.org/10.1093/brain/awp270.
Whitney, C., Kirk, M., O'Sullivan, J., Lambon Ralph, M.A., Jefferies, E., 2011. The neural organization of semantic control: TMS evidence for a distributed network in left inferior frontal and posterior middle temporal gyrus. Cereb. Cortex 21 (5), 1066–1075. https://doi.org/10.1093/cercor/bhq180.
Whitney, C., Kirk, M., O'Sullivan, J., Lambon Ralph, M.A., Jefferies, E., 2012. Executive semantic processing is underpinned by a large-scale neural network: revealing the contribution of left prefrontal, posterior temporal, and parietal cortex to controlled retrieval and selection using TMS. J. Cogn. Neurosci. 24 (1), 133–147. https://doi.org/10.1162/jocn_a_00123.
Xu, Y., He, Y., Bi, Y., 2017. A tri-network model of human semantic processing. Front. Psychol. 8. https://doi.org/10.3389/fpsyg.2017.01538.